

Understanding Radiation Flow in a Stochastic Medium

CHRISTOPHER L. FRYER,¹ PAUL A. KEITER,² VIDUSHI SHARMA,¹ JOSHUA LEVEILLEE,¹ D.D. MEYERHOFER,²
D. H. BARNAK,³ TOM BYVANK,² A. T. ELSHAFIEY,² CHRISTOPHER J. FONTES,^{1,2} HEATHER M. JOHNS,²
P. M. KOZLOWSKI,² AND TODD URBATSCH²

¹*Center for Theoretical Astrophysics, Los Alamos National Laboratory, Los Alamos, NM, 87545, USA*

²*Los Alamos National Laboratory, Los Alamos, NM, 87545, USA*

³*Laboratory for Laser Energetics, University of Rochester, NY, 14623, USA*

Submitted to ApJ

ABSTRACT

Radiation flow through an inhomogeneous medium is critical in a wide range of physics and astronomy applications from transport across cloud layers on the earth to the propagation of supernova blast-waves producing UV and X-ray emission in supernovae. This paper reviews the current state of the art in the modeling of inhomogeneous radiation transport, subgrid models developed to capture this often-unresolved physics, and the experiments designed to improve our understanding of these models. We present a series of detailed simulations (both single-clump and multi-clump conditions) probing the dependence on the physical properties of the radiation front (e.g. radiation energy) and material characteristics (specific heat, opacity, clump densities). Unless the radiation pressure is high, the clumps will heat and then expand, effectively cutting off the radiation flow. The expanding winds can also produce shocks that generates high energy emission. We compare our detailed simulations with some of the current subgrid prescriptions, identifying some of the limitations of these current models.

Keywords: radiative transfer — supernovae — laboratory astrophysics — radiative transfer simulations

1. INTRODUCTION

For many physics and astrophysics applications, energy transport is often carried by photons, neutrinos and electrons. In its generality, solving this energy transport problem requires modeling a seven dimensional problem where the spatial, angular and energy distribution of these carriers must be evolved (see reviews <https://www.osti.gov/servlets/purl/917504>). Coupling this energy transport to matter drives further hydrodynamic instabilities, pushing the limits of our current modeling capabilities. This has led to many approximate methods in modeling radiation-hydrodynamics that include simplifications in the radiation transport (e.g. integrating over angle or energy), coupling terms (e.g. modeling pure transport or pure hydrodynamics models), or spatial dimensions (homogenizing the radiation flow into a 1-dimensional flow). These simplifying assumptions are all valid in specific conditions. For example, for supernova shocks traveling within a star, radiation is trapped in the flow, but after the shock breaks out of the star well into the circumstellar medium, radiation flows freely from where it is emitted and the hydrodynamics can be approximated by a simple homologous outflow. In stars, although the radiation is not trapped, it is in the “diffusive” regime where the angular distribution is well-defined and integrating over angle can remove dimensions from the numerical problem.

Although many studies exist that investigate different approximations in radiation transport or radiation-hydrodynamics coupling, there are far fewer studies of the role of inhomogeneities in energy transport (also known

as heterogeneous transport or transport through a clumpy medium). The effect of a clumpy medium can modify transport solutions across a broad range of approximation regimes. In transport-only solutions, inhomogeneous media can alter the angular distribution of the radiation. In optically thin applications, these more optically-thick clumps screen the photons, reducing the radiative flux. In more optically-thick regimes, they alter the radiation flow. In radiation-hydrodynamics calculations, a broad range of additional physical effects from radiation/clump interactions can alter the radiative flow. Radiation can cause ablation or, through heating, drive a wind from the clumps. In this paper, we refer to ablation when the disruption of the material is due to momentum deposition and “blow-off” or “wind” when the outflow is due to energy injection. This can inject higher density and, in some cases, higher opacity material into the surroundings, increasing the impact of the clumps on the radiation flow. Shocks from these winds can produce high-energy emission, altering the energy spectrum of the radiation. In some cases, radiative pressure can cause the clumps to implode. The importance of these different effects depends on the applications and their conditions.

This paper investigates the radiation flow through these clumpy media, studying the physics effects on the radiation transport and coupling between radiation and hydrodynamics. Understanding the details of radiation flow in clumpy media will enable a better use of observations in nature and results from high energy-density experiments to constrain and validate simulations (codes, numerical methods, physical data, models, and the approximations therein). Although becoming less rare, modeling a clumpy medium at scale severely strains computational resources, even on massive supercomputers. In addition to the aforementioned numerical approximations, simplifications include simulating a small subset of the medium and homogenizing or under-resolving small geometric details. An under-resolved simulation tests the asymptotic behavior of the numerical methods and the accuracy of averaging methods for geometry, materials, equations of state, and opacities. Furthermore, a clumpy medium that we simulate or fabricate for an experiment is usually a single and particular realization of a stochastic medium, which is defined probabilistically. Transport-in-Stochastic-Media methods have been developed to produce ensemble-average linear transport solutions, as if an infinite number of simulations of media sampled from the stochastic definitions were run and averaged. The applications of these methods to coupled radiation-hydrodynamics are much less mature, as is an accompanying estimation of the standard deviation of the ensemble average. For the bulk of this paper, we focus on energy transport via photon radiation. Many of the conclusions also apply to other energy carriers including neutrinos and electrons scaled by the transport regime (mean free path) and emission/deposition properties. Section 2 reviews a set of applications where radiative transport through an inhomogeneous medium is important, discussing which physical effects are most critical in each application. Section 3 reviews the current state of both modeling and experiment to study inhomogeneous radiation flow. In this paper, we focus on detailed radiation-hydrodynamics calculations to better understand the physics behind radiation flow and Section 4.1 describes our initial conditions and the computational methods used in this paper. Section 4.2 focuses on the basic physics behind radiation flow across a single clump. Section 4.3 studies the more complex interactions in a multi-clump medium. We conclude with a discussion of how the physics studied in these simulations affects the different applications.

2. APPLICATIONS

Radiation transport is critical in a wide range of applications including oncological treatments, radiation shielding, nuclear reactors, astrophysics, and planetary atmospheres; for a review, see (Byvank et al. 2024).

In some cases (particularly in astrophysics), the deposition of energy and momentum from this radiation plays a critical role in the evolution of the phenomena. For example, momentum deposition from radiation is key in understanding mass outflow from stars. Astronomers are now realizing that the smooth, line-driven winds (Puls et al. 2008) are too simple to explain all of the features in the stellar wind profile. Explosive shell burning, opacity-driven instabilities and pressure waves can all produce bursts of mass ejection in a star, producing inhomogeneities in the circumstellar medium including both shells and clumpy media (Fryer et al. 2006; Herwig et al. 2014; Quataert et al. 2016). Studies of line-driven winds indicate that even these, relatively quiescent, outflows, can produce large inhomogeneities in the circumstellar medium (Owocki & Rybicki 1984; Puls et al. 2008; Sundqvist et al. 2018; Jiang et al. 2018; Owocki et al. 2019). In particular, clumping in the line-driven wind can alter the radiation and mass outflow from these winds (Sundqvist et al. 2018; Owocki & Sundqvist 2018). Understanding the interaction between radiation and these clumps determines both this mass loss and the evolution of these clumps.

The clumpy structure produced in stellar winds provides the initial conditions through which supernova explosions propagate. Radiation is typically trapped in the material shock until the supernova breaks out of the star. It is

believed that the edge of the star is marked by a sharp density break as the stellar profile transitions to a stellar wind profile. In simple spherically symmetric models, the radiation in the shock rapidly transitions from being trapped in the material flow to freely streaming out of the shock (Waxman & Katz 2017). This effect depends sensitively on the structure of the edge of the star as well as asymmetries in the supernova blastwave (from the explosion and the stellar envelope) which complicate this picture (Bayless et al. 2015; Lovegrove et al. 2017; Fryer et al. 2020a; Irwin et al. 2021). Especially in Wolf-Rayet stars where shock breakout actually occurs in the wind, not the edge of the star, shock breakout can be drastically modified by the radiation flow through the clumpy wind material (Fryer et al. 2020a). Interactions between the radiation and the clumps disrupt the clumps and the ablation of these clumps produce shocks that drive high-energy emission (Fryer et al. 2020a).

Beyond shock breakout, interactions of the radiation flow with the circumstellar medium can dramatically alter the observed supernova light-curves. Interactions of the radiation with the circumstellar medium drive many of the features seen in type II narrow-line supernovae. Most of the current studies focus on the interaction with a spherically symmetric shell (e.g. Roming et al. 2012), but it is likely that the circumstellar medium is much more heterogeneous.

Transport of radiation through a dusty medium is another application where including the inhomogeneities of the clumps (dust particles) can alter the propagation of radiation and albedo of a dust cloud (Boisse 1990; Witt & Gordon 1996, 2000; Hegmann & Kegel 2003). This phenomenon plays a role in analyzing observational data of these dust clouds, the penetration of energy in molecular clouds, and the destruction of dust. These effects, in turn, can alter star formation in molecular clouds. The propagation of radiation around dense clumps in molecular clouds can cause the clumps to implode, driving star formation (Klein et al. 1980; Sandford et al. 1982; Bisbas et al. 2011; Proga et al. 2014). This inhomogeneous transport should also affect the interpretation of nova and supernova observations, but less work has been done in this field.

Climate and environmental studies have also studied inhomogeneous radiation flow. Understanding the transport through vegetation canopies is important both for agriculture and climate modeling (Kassianov 2003; Shabanov et al. 2007). Climate scientists have studied radiative transfer through inhomogeneous cloud cover (Cook et al. 2004; Hogan et al. 2016) and recipes to mimic that transfer are used in many climate codes (Wu 2013; Hogan et al. 2016). With improving satellite data, tests of these models become increasingly stringent, driving advances in this transport.

Studies of transport through an inhomogeneous or stochastic medium is not limited to photons. A growing number of charged particle transport studies, particularly of cosmic rays (high energy electrons, protons and ions), have focused on the radiation flows across single clumps (Wiener et al. 2019; Bustard & Zweibel 2021) and turbulent media (Huang et al. 2022). These studies focused both on the effect of the clumpy media on the flow of radiation and the effect of the radiation on the clumps, including the energy and momentum deposition of the radiation into the clumpy media.

3. CURRENT UNDERSTANDING

3.1. *Inhomogeneous Transport Solutions*

The effects of radiation transport through inhomogeneous media depends on the properties of the inhomogeneities. Studies of inhomogeneities generally consider a 2-component medium consisting of a radiation flow region with embedded clumps. Throughout this paper, we will refer to the “flow” region as the lower-density region through which the radiation front propagates, and the clump region as the denser clumps around which the radiation flows. In experiments, the flow region is often composed of a silicate foam and the clumps are inclusions in that foam. In many astrophysical applications, the flow region is simply the lower density region where the clumps are produced by dense turbulent eddies. The effect of the clumps depends on their densities, opacities, specific heats, geometry, sizes, and covering fractions. It depends on the transport regime: diffusion limit, transport regime, free-streaming limit of the radiation flow. In the free-streaming limit, dense clumps can completely alter the nature of the flow. For instance, inhomogeneities in atmospheric clouds can lead to an increase in the albedo of the cloud layer, decreasing the amount of radiation that reaches a planet’s surface. In the diffusive regime, radiation is more able to flow around clumps. Transport-regime conditions lie in between these two extremes.

Many of the solutions developed for radiation transport in inhomogeneous media are most appropriate in the diffusion limit. These methods often use Markov-process solutions (Vanderhaegen 1986; Malvagi et al. 1989; Su & Pomraning 1994, 1995; Smith 2003; Kassianov 2003; Olson et al. 2006; Olson 2007; Davis & Xu 2014) with Poisson distributions of the inhomogeneities. Some studies derived solutions assuming specific properties of the inhomogeneities (Vanderhaegen 1988). Other studies focused on understanding the solution limits (Malvagi et al. 1989; Miller et al. 2001). The simplifications required in these analytic or semi-analytic solutions drove scientists to develop in-

creasingly sophisticated modeling tools to capture radiation-flow in heterogeneous media (Brantley 2011; Vu et al. 2020; Larmier et al. 2021). Many of the studies focused on developing reduced-order models that rely on a subset of the relevant physics (e.g. mean free path with respect to clump size, number density of clumps, clump spacing, etc.).

A straightforward approach to introduce inhomogeneities in reduced order techniques is to derive an effective opacity in the region with inhomogeneities. For example, the approach of Prinja & Olson (2005); Olson (2007) included an additional effective scattering opacity as well as a modification to the absorption opacity for an inhomogeneous medium for a purely absorptive medium. The effective absorption opacity ($\sigma_{a,\text{eff}}$) is given by:

$$\sigma_{a,\text{eff}} = 1/(p_1/\sigma_{a1} + p_2/\sigma_{a2}) \quad (1)$$

where $p_{1,2}$ are the covering fractions or covering fractions of the clump and surrounding medium respectively and $\sigma_{a1,a2}$ are the equivalent absorption opacities for these materials. They included an effective scattering opacity ($\sigma_{s,\text{eff}}$):

$$\sigma_{s,\text{eff}} = \nu^2/[\tilde{\sigma}(1 + \lambda_c\tilde{\sigma})] \quad (2)$$

where $\tilde{\sigma} = p_1\sigma_{a1} + p_2\sigma_{a2}$ is the average opacity, $\nu^2 = p_1p_2(\sigma_1 - \sigma_2)^2$, and $\lambda_c = \lambda_1\lambda_2/(\lambda_1 + \lambda_2)$ is the geometric mean of the chord lengths, where the chord length is defined by the length of a chord covered by each material.

Using this prescription, we can calculate the effective absorption and scattering opacities as a function of the covering fraction of the clumps. Figure 1 shows the effective absorption and scattering opacities under this formalism as a function of the clump covering fraction. Although the effective absorption cross section does not increase until the clump covering fraction is large, the effective scattering term quickly approaches the value of the clump opacity. This scattering term can drastically lower the propagation speed of the radiation.

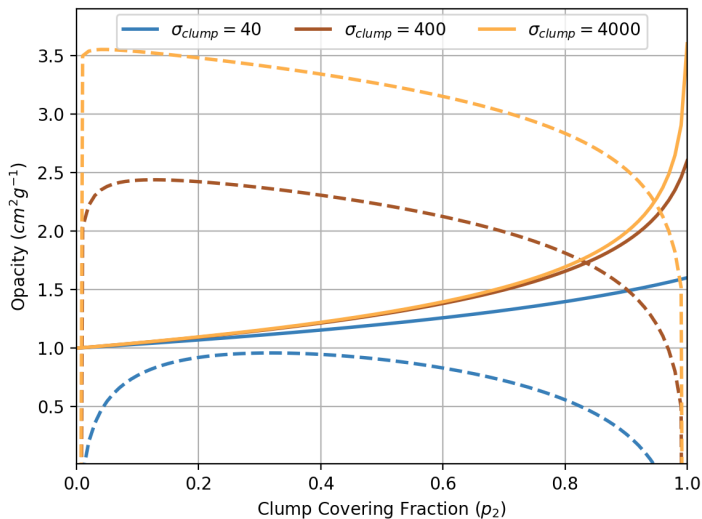


Figure 1. Effective absorption (solid) and scattering (dashed) opacities for three values of clump opacity (in $\text{cm}^2 \text{g}^{-1}$) as a function of clump covering fraction. The opacity of the flow region is $10 \text{ cm}^2 \text{g}^{-1}$ and the density of the flow, clump regions are 0.05 g cm^{-3} , 5 g cm^{-3} respectively. The effective absorption opacity does not increase significantly until the covering fraction exceeds 0.8. However, the effective scattering opacity can be high if the clump opacity is high compared to the opacity in the flow region.

For stellar winds, Sundqvist et al. (2014) used a different approach, setting the opacity to

$$\sigma = \tilde{\sigma}(1 + \tau_{\text{cl}}f_{\text{ic}})/(1 + \tau_{\text{cl}}) \quad (3)$$

where τ_{cl} is the clump optical depth and f_{ic} is the density of the inter-clump medium divided by the average density of the medium.

Most of these past studies focused on transport-only solutions or solutions where radiation/hydrodynamic effects can be minimized. As such, the solutions typically only consider the relative opacities of the different clumps. More

detailed studies included the effects of the size scale of the clumps (with respect to the photon mean free path). This effect becomes increasingly important as we move from the diffusive to the free-streaming transport regimes.

3.2. Experiments

A number of experiments studying radiation transport in clumpy media already exist. [Shaoen et al. \(2005\)](#) performed experiments investigating supersonic radiation propagation in a low-density heterogeneous medium. These experiments investigated radiation propagation in a low-density plastic (C_6H_{12}) foam target as well as in a Cu-doped foam ($C_6H_{12}Cu_{0.394}$). The Cu was added by means of small (59 nm in diameter) Cu particles and achieved roughly a 2.14% atomic fraction. The foams were viewed face-on with a trichromatic streaked x-ray spectrometer (TCS). The TCS consisted of a three-imaging-pinholes array and a three-transmission-grating array coupled with an x-ray streak camera. The TCS observed the emission from two different photon energies, 210 eV and 840 eV. A soft x-ray spectrometer observed the soft x-ray spectrum of the hohlraum, from which a temperature could be inferred. Finally, a transmission grating spectrometer was used to measure the time-integrated spectrum from either the hohlraum or the foam sample. A delay in the radiation breakout was observed when comparing the Cu-doped foam with the pure foam case for emission at 210 eV; however, this trend was reversed when comparing emission at 840 eV. The opacity for both the pure foam and the Cu-doped foam was estimated at each of these energies. For the pure foam, the opacity was determined to be $273 \text{ cm}^2/\text{g}$ and $407 \text{ cm}^2/\text{g}$ for x-rays of energy 210 eV and 840 eV, respectively. For the Cu-doped foam, the opacity was determined to be $967 \text{ cm}^2/\text{g}$ and $760 \text{ cm}^2/\text{g}$ for 210 eV and 840 eV photons, respectively. This study concluded that differences in the opacities caused the different measured radiation flow speeds. But as we shall see here, the flow may also depend on the blow-off of the inclusions in the flow region.

More-recent experiments by [Keiter et al. \(2008\)](#) examined radiation with multiple particle sizes. These experiments used a gold hohlraum as a radiation source to drive a supersonic heat wave into a foam package. The inhomogeneous medium was a low-density ($65 \text{ mg}/\text{cm}^3$) plastic foam $C_{15}H_{20}O_6$ with Au particles. The Au fraction from the particles ranged from 0 to 14% by atomic fraction. This type of characterization allows one to visualize the distribution of Au particles throughout the foam and to determine if the particles are clumping together, thereby resulting in a different distribution than originally thought. As we shall see in [Section 4.3](#), characterization of these foams is absolutely crucial for understanding the radiation transport. A detailed description of the complete characterization of these particular foams is found in [Keiter et al. \(2008\)](#).

Three different regimes were studied in these experiments, corresponding to no particles (or the homogeneous situation) and particles that are sub-micron and 6 microns in diameter. The position of the radiation front was measured by observing the self-emission of the foam with a soft x-ray imager [Ze et al. \(1992\)](#). The soft x-ray imager observed a narrow bandwidth of radiation, peaking around 270 eV. The position of the radiation front was measured in each experimental case and compared with simulations. It should be noted that while foam packages were observed face-on in many previous radiation flow experiments, these measurements were made side-on in order to allow multiple measurements to be made and a time history to be compiled.

In order to demonstrate the ability to correctly simulate and understand the radiation propagation with this particular foam, measurements were first obtained with a homogeneous foam. Next, measurements of the position of the radiation front were made in inhomogeneous foams and then compared with two types of simulations: simulations of the pure foam case and simulations using an atomic-mix model. Although the atomic-mix model matches the smallest particles well, neither model could explain the radiation front position for the 6 micron diameter particles. The Pomraning model ([Pomraning 1998](#)), a precursor to the model described in [Section 3.1](#), was then applied to the simulations. This model assumed a mean particle size of 6 microns in diameter and the particles were in pressure equilibrium with the foam. The mean opacity was determined based on the material properties at each timestep in the calculation. The mean opacity was then divided by the opacity of the homogeneous foam to determine a correction factor to apply. This correction factor depended on the temperature of the Au-foam mixture and therefore changed in time as the temperature of the system evolved. Within the uncertainties of these experiments, the Pomraning model provided a good fit to the data.

4. PHYSICS OF INHOMOGENEOUS FLOWS

In this section, we present a wide set of calculations of radiation flow across an inhomogeneous medium, using simplified conditions to better understand the physics. [Section 4.1](#) discusses the basic models used followed by two sections focusing on single- ([Section 4.2](#)) and multi-clump ([Section 4.3](#)) physics effects.

4.1. *Simulation Tools and Initial Conditions*

For our calculations, we use conditions close to that of the XFOL and XFLAWS experimental campaigns led by LANL (Johns et al. 2023; Byvank et al. 2024) and the *Cassio* code developed under LANL’s Advanced Simulation and Computing program. The *Cassio* code models hydrodynamics using a cell-based adaptive mesh refinement scheme with a two-shock approximate Riemann solver. The code has been verified against a variety of analytic test problems, the most relevant for this problem being the Sedov blast wave (Gittings et al. 2008). Radiation transport can be modeled using a variety of transport solutions including flux-limited diffusion (Gittings et al. 2008), discrete ordinate (S_N) (Fryer et al. 2020a), and Implicit Monte Carlo transport (Urbatsch & Evans 2006).

The *Cassio* code has been used extensively in the laboratory experimental community for a wide variety of problems studying hydrodynamics or radiation-hydrodynamics (e.g. Johns et al. 2016; Falk et al. 2017, 2018, 2020a; Fryer et al. 2020b; Falk et al. 2020b; Johns et al. 2021; Coffing et al. 2022; Johns et al. 2023; Fryer et al. 2023). In addition to many of these validation tests, the *Cassio* has been verified against other experimental codes (e.g. Fatenejad et al. 2013; Falk et al. 2014). It has been applied to a number of radiation-hydrodynamics problems in astrophysics (for a review, see Fryer et al. 2020a) and has been verified against other astrophysical codes as well (Joggerst et al. 2014).

For most of our calculations, we use *Cassio*’s S_N transport scheme with an $N = 8$ quadrature set and 71 energy groups. The coarse grid resolution is $0.6 \mu\text{m}$ and we use only 2 levels of refinement. We discuss comparisons to other transport schemes and grid resolutions below.

The initial conditions for our simulations are guided by active XFOL and XFLAWS experimental campaigns (Johns et al. 2023; Byvank et al. 2024) that builds upon past Pleiades and COAX radiation flow studies (Fryer et al. 2020b; Johns et al. 2021; Coffing et al. 2022). In these experiments, a laser-driven hohlraum (either at the Omega laser facility in Rochester (Boehly et al. 1995) or the National Ignition Facility at Lawrence Livermore National Laboratory (Haynam et al. 2007) produces a radiation front that then propagates through a target. This experiment consists of a target placed on top of a hohlraum (Figure 2). Lasers fired into the hohlraum create a hot, radiation-dominated plasma that then propagates through the experimental target. The power in this drive peaks quickly and then decays slowly over the course of our few-ns simulation. In our multi-clump, high-drive models, we also consider a simplified flat power (or temperature) for this drive. The target is a silicon dioxide foam filled with vanadium-oxide inclusions; the opacities are obtained from the OPLIB database (Colgan et al. 2016), calculated with the Los Alamos suite of atomic physics codes (Fontes et al. 2015). In this paper, we focus solely on modeling the target, using a radiation source term at its base to represent the hohlraum-produced radiation flow. The target is modeled in cylindrical symmetry with a radius of 0.04 cm and a height of 0.08 cm.

4.2. *Single Clump Studies: Probing the Fundamental Physics*

The interaction of a radiation flow with a clumpy medium has much broader effects than the alteration of the flow of radiation including outflows and shocks. The magnitude of these effects depends upon the properties of the clumps. To understand this physics, we have conducted a number of focused, single clump radiation studies. For these studies, we use our standard experimentally-motivated target (Section 4.1) with a single embedded clump. These single-clump simulations allow us to study the physical effects and the dependencies of these effects on the properties of the clumps.

As a first study, we focus on the effects of clump density. Figure 3 shows the density map of 4 separate simulations 1.6 ns after the launch of the radiation front where the only difference in the 4 simulations is the density of the clump. For these clumps, the composition of clump and flow regions are identical. Only the clump density is varied including models where the clump density is lower and higher than the ambient flow region density. For the low-density clump, radiation rushes through the cavity, leading the flow in the ambient region. For high density clumps, the radiation flows around the clumps. For modest density increases (e.g. 10 times the ambient medium), the radiation can both ablate and compress the clump. However, the timescale to do this increases with increasing clump density and, at the snapshot in time shown in Figure 3, the radiation flow has little effect on the clump.

The radiation heats up the clump, striving to place it in temperature equilibrium. If the clump is denser than that of its surroundings, it begins to blow a wind, sending a material flow back into the flow region. As we shall discuss below, if the composition of the clumps is different than the ambient medium, these outflows mix into the flow region. If this material has higher opacity, it can choke off the radiation flow. Another features of these outflows is that they can cause shocks, raising the temperature of the outflow (Figure 4). These shocks are critical in understanding supernova outflows, producing extended Ultraviolet and X-ray emission (Fryer et al. 2020a). The alterations in the flow caused by a low-density region can also alter the temperature profile. Especially in ambient media where the

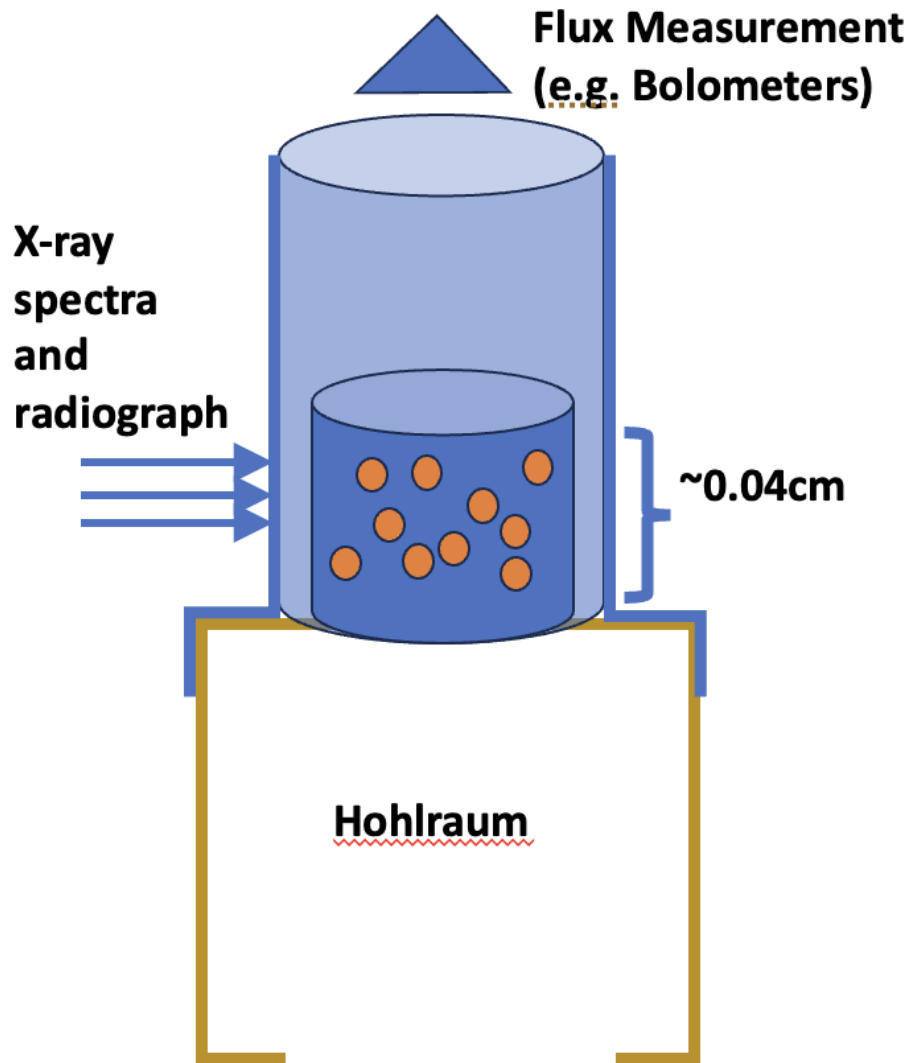


Figure 2. Simplified diagram of the experiment XFOLE experiment (Johns et al. 2023) designed to measure radiation flow through an inhomogeneous medium. Lasers heat the gold-line hohlraum cavity, producing a hot plasma that drives a radiation front through a target. Dense inclusions are added into a low-density foam target that is roughly 0.04 cm in size. The radiation front can be probed both using a radiograph to measure the position of the front or a spectrograph to constrain the temperature and composition. The escape of the radiation front from the top of the target can be used to measure the radiation flux versus time.

radiation is in the transport or free-streaming regime, this heating from radiation-matter interactions can dramatically alter the emerging spectra. If the radiation flow is highly photon-energy dependent, this effect can also alter the flow of radiation.

Matter interactions are important in our simulations. They drive outflows that both heat the material, altering the energy distribution of the radiation, and inject clump material into the ambient medium. The physics behind these outflows can be understood through pressure and energetic constraints. Radiation heats the clumps, striving to achieve temperature equilibrium. But, as soon as the pressure in the clump exceeds the radiation dominated gas, it will expand. The pressure in the clump/flow region can be approximated by a combination of ideal gas and radiation

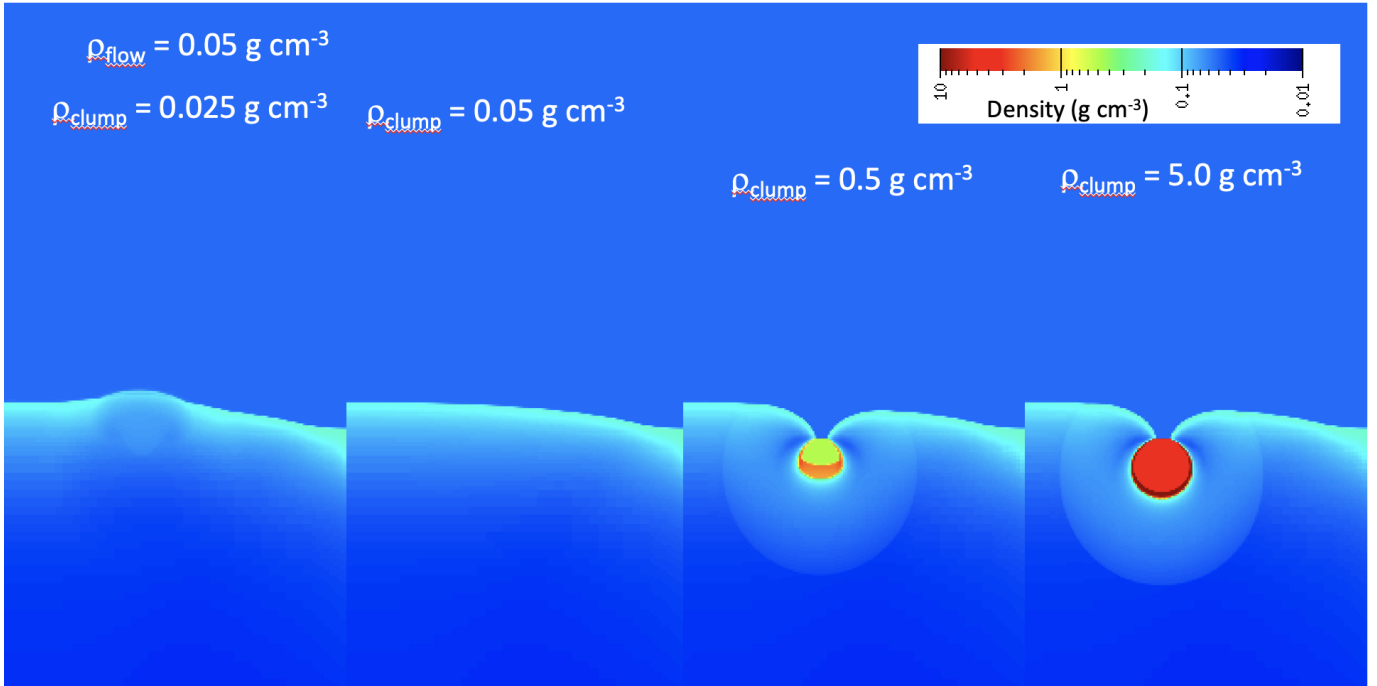


Figure 3. Density map for 4 cylindrical models after 1.6 ns where the clump density is varied (left to right) from 1/2 of the flow region density to 100 times the flow region density. The opacity varies dramatically as the radiation front sweeps down the flow region. For the cold material, the initial Rosseland opacity for the low-energy X-ray photons in this flow is $> 4 \times 10^4 \text{ cm}^2 \text{ g}^{-1}$. Once heated, the opacity drops by over an order of magnitude and the mean free path in the foam region is roughly 0.01 cm and the flow region is roughly 8 mean free paths long. The clump opacity is roughly 50% higher. In the high density clump (roughly the density used for most of our calculations), the mean free path is 0.03–0.1 μm and since the bulk of the clump remains cold throughout the calculation, this mean free path remains low.

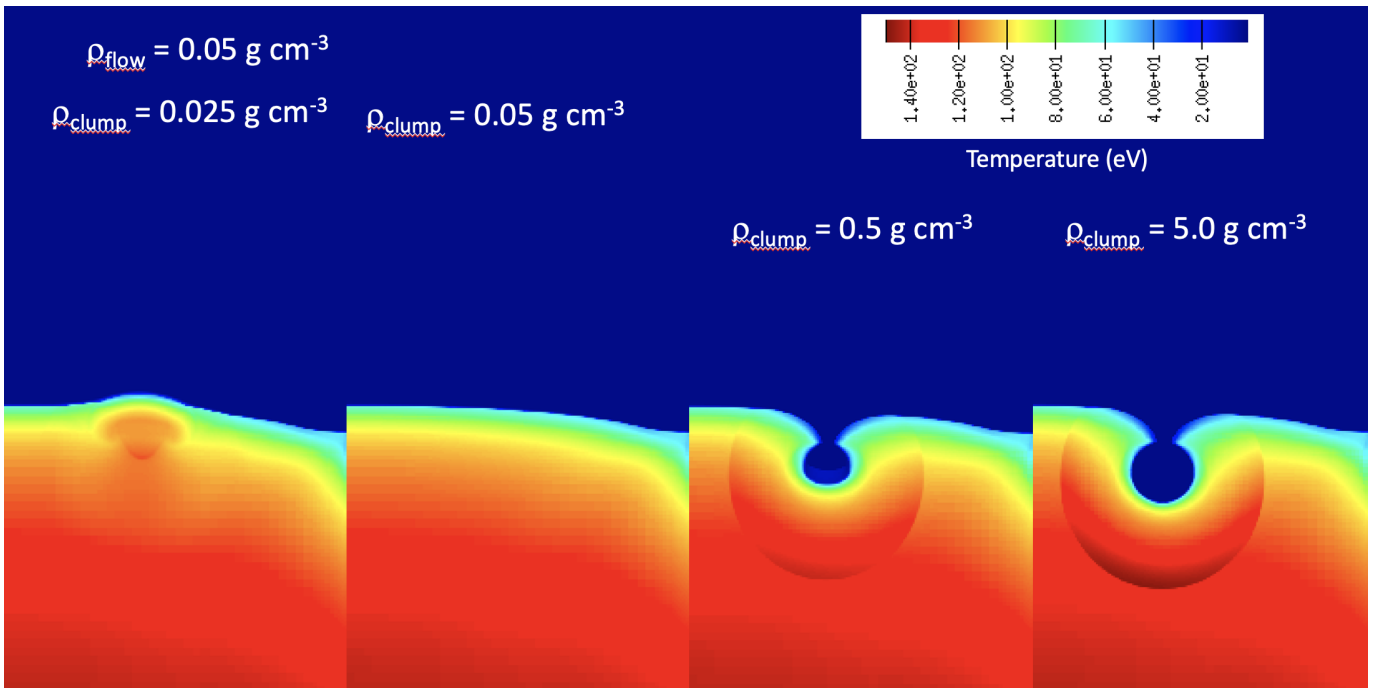


Figure 4. Temperature map for 4 cylindrical models after 1.6 ns where the clump density is varied (left to right) from 1/2 of the flow region density to 100 times the flow region density (same as Figure 3).

pressure:

$$P_{\text{clump/flow}} = \rho_{\text{clump/flow}} / \langle A \rangle R T_{\text{clump/flow}} + a_{\text{rad}} / 3T_{\text{clump/flow}}^4 \quad (4)$$

where $P_{\text{clump/flow}}$, $\rho_{\text{clump/flow}}$ and $T_{\text{clump/flow}}$ are the pressure, density and temperature of the clump or flow region, $\langle A \rangle$ is the average atomic weight of the material, $R = 8.31 \times 10^7 \text{ erg K}^{-1} \text{ mol}^{-1}$ is the universal gas constant, and $a_{\text{rad}} = 7.567 \times 10^{-15} \text{ erg cm}^{-3} \text{ K}^{-4}$ is the radiation constant. Figure 5 shows the clump temperature versus the flow-region temperature when the pressure in the clump equals that of the flow region. The lines in this plot denote pressure equilibrium at the two temperatures on the x and y axes. We have set up rough conditions for our experiment where $\rho_{\text{clump/flow}} / \langle A \rangle = 0.01$ and we vary the clump value up to 30 times higher. At these densities, ideal gas pressure dominates the radiation pressure at the temperatures in the experiment. As the clump is heated, its pressure will exceed that of the flow region and it will expand, blowing a wind into the flow region.

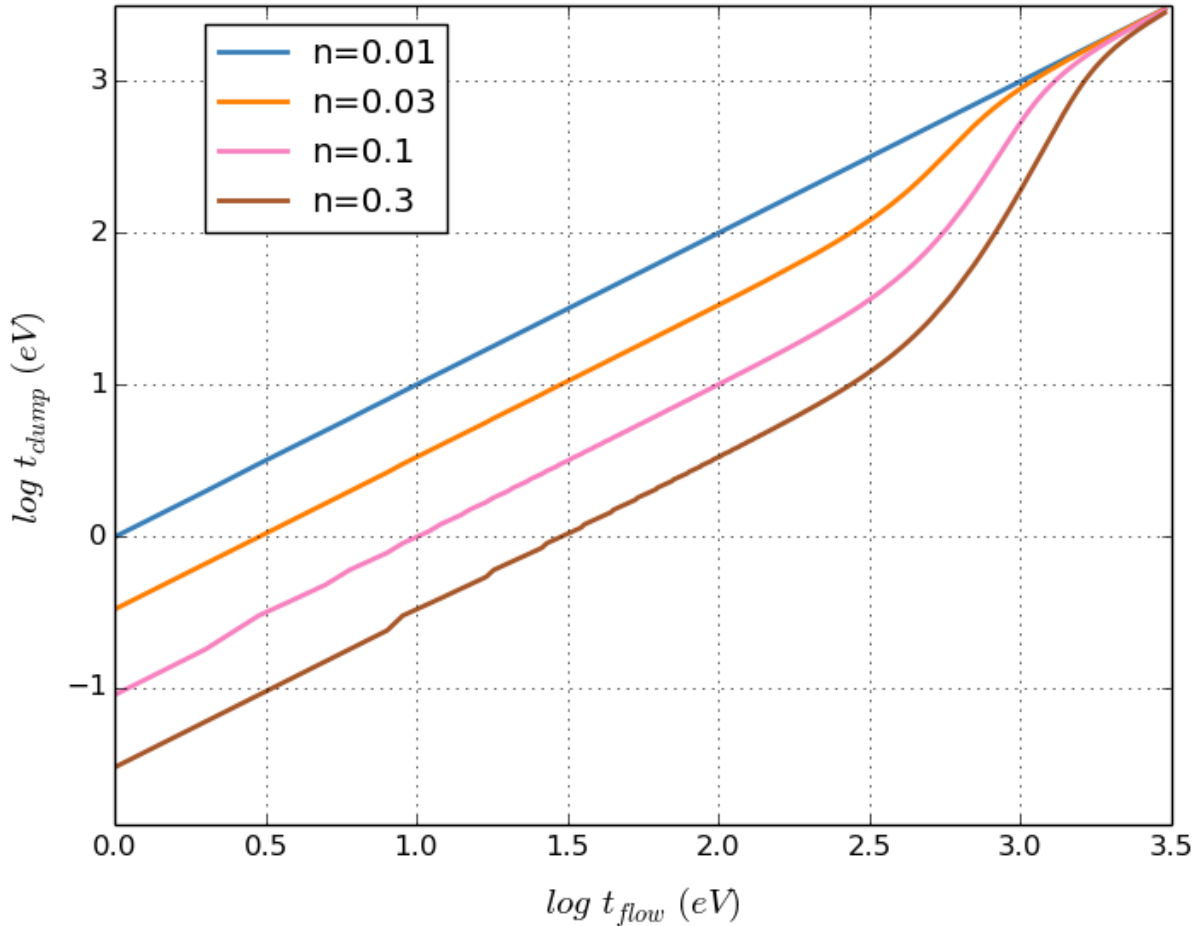


Figure 5. Curves of pressure equilibrium versus the temperature of the flow region (x axis) and the temperature in the clump (y axis). In this scenario, we assume $\rho_{\text{flow}} / \langle A \rangle$ for the flow region is 0.01 mol cm^{-3} and vary the quantity $n = \rho_{\text{clump}} / \langle A \rangle$ over four different values. These conditions are reasonably close to those in our laboratory experiment.

If the radiation pressure dominates (at roughly 1–3 keV for these conditions), the blow-off is likely to be minimal. For many astrophysical applications, the density of the material is lower and the temperature at which radiation dominates will also be lower. The critical temperature (T_{crit}) can be estimated by assuming that radiation pressure dominates the flow region and determining the temperature in an ideal gas to match that pressure, i.e.

$$T_{\text{crit}} = a_{\text{rad}} / 3T_{\text{flow}}^4 / (\rho_{\text{clump}} / \langle A \rangle R). \quad (5)$$

Phenomena	$\rho/\langle A \rangle$	T_{crit}	T_{flow}	Dominant Pressure
Stellar Wind				
$dM/dt = 10^{-7} M_{\odot} \text{y}^{-1}$, radius = 10^{13} cm	$5 \times 10^{-17} \text{ mol cm}^{-3}$	200 K	10,000 K	Radiation
$dM/dt = 10^{-6} M_{\odot} \text{y}^{-1}$, radius = 10^{12} cm	$5 \times 10^{-13} \text{ mol cm}^{-3}$	2,000 K	10,000 K	Radiation
Wolf-Rayet Wind				
$dM/dt = 10^{-5} M_{\odot} \text{y}^{-1}$, radius = 10^{12} cm	$5 \times 10^{-13} \text{ mol cm}^{-3}$	4,500 K	20,000–200,000 K	Radiation
$dM/dt = 10^{-3} M_{\odot} \text{y}^{-1}$, radius = 10^{12} cm	$5 \times 10^{-11} \text{ mol cm}^{-3}$	20,000 K	20,000–200,000 K	Radiation
$dM/dt = 10^{-3} M_{\odot} \text{y}^{-1}$, radius = 10^{11} cm	$5 \times 10^{-9} \text{ mol cm}^{-3}$	90,000 K	20,000–200,000 K	Rad/Mat
$dM/dt = 10^{-1} M_{\odot} \text{y}^{-1}$, radius = 10^{12} cm	$5 \times 10^{-9} \text{ mol cm}^{-3}$	90,000 K	20,000–200,000 K	Rad/Mat
Molecular Clouds	$1.7 \times 10^{-19} \text{ mol cm}^{-3}$	30 K	10 K	Mat/Rad
Clouds	$0.056 \text{ mol cm}^{-3}$	1.8 keV	1 eV	material

Table 1. Dominant pressure term for different applications. Even though radiation dominates many of the applications, we note that blow-off of the clumps may still play a key role in the evolution (see Section 4.3).

Table 1 provides rough values of the critical temperature above which radiation pressure dominates and this blow-off is minimized. For the different phenomena, both the clump density and temperature of the flow region can vary by many orders of magnitude. For most stars, high stellar radii and low mass-loss rates lead to conditions where the stellar radiation dominates the pressure. Even though Wolf-Rayet stars are hotter, the mass loss rates are higher and the stars are more compact. Near the stellar surface, material pressure can be important.

The specific heat of the clump material dictates the amount of energy that must be injected into this material to heat it ($\Delta T \propto \Delta E/c_v$: the change in temperature is proportional to the change in energy divided by the specific heat). This will determine both how quickly the clump begins to expand or blow off as well the temperature of this blow-off. The higher the specific heat, the longer it takes for the radiation and material temperatures to reach an equilibrium. The specific heat dictates the timescale for the temperature in the clumps to rise. Because the opacity is extremely sensitive to the temperature, the specific heat can play a huge role in determining the evolution of the opacity in the flow.

From our analytic models, we expect the outflows to depend upon both the specific heat and opacity of the material. Figure 6 shows the temperature map from two simulations at two snapshots in time where the specific heat is raised and lowered by an order of magnitude. For high specific heat models, the temperature in the clump need only rise modestly to achieve sufficient pressures to push out against the ambient medium, driving an outflow into the flow region. If the clump material has a lower specific heat, it must become hotter to achieve the requisite pressures to drive an outflow. The outflow will take longer to expand and will be hotter.

Figure 7 shows the density and volume fraction (f_{vol}) maps corresponding to the temperature maps in Figure 6. Because the outflow starts earlier for the higher specific heat model, it expands more quickly into the ambient medium. In addition to being lower temperature, the density of the outflow is lower for higher C_v clump. If the opacity of this material is high, it can cut off the radiation flow. Although the high specific clump material expands more quickly, it is less dense, so the impact on the radiation flow may be greater for the clumps with lower specific heats.

The opacity of the clump material can modify the evolution of the clump. Figures 8 and 9 show the density, temperature, opacity and volume fraction for models where the opacity of the clump material is raised or lowered. If the opacity of the clump is high, the radiation is unable to penetrate deeply into the clump. This means that the wind from the clump taps only a small mass reservoir. The resulting outflow is lower density but higher temperature. The extent of the high-opacity outflow is slightly lower. Depending on how the opacity evolves as it transitions from a solid to a plasma, the nature of the clump-material opacity can have a huge impact on the radiation flow.

One important aspect of many computational studies of transport in inhomogeneous media is that all opacity databases that we are aware of assume that the material is a plasma. Especially for laboratory experiments, the embedded clumps are in a solid phase, and the opacity of this material can be very different from opacities obtained under plasma conditions. Electrons obey Fermi-Dirac statistics, which ensures that at solid densities, the partial occupation of higher-lying energy levels decays slowly, resulting in the long characteristic Fermi-Dirac tail. However in dense plasmas, the eigenspectrum is continuous and the partial occupations die out rapidly. This behavior governs the intra (inter) band transitions, or equivalently, bound-bound, bound-free, and free-free electron transitions, and

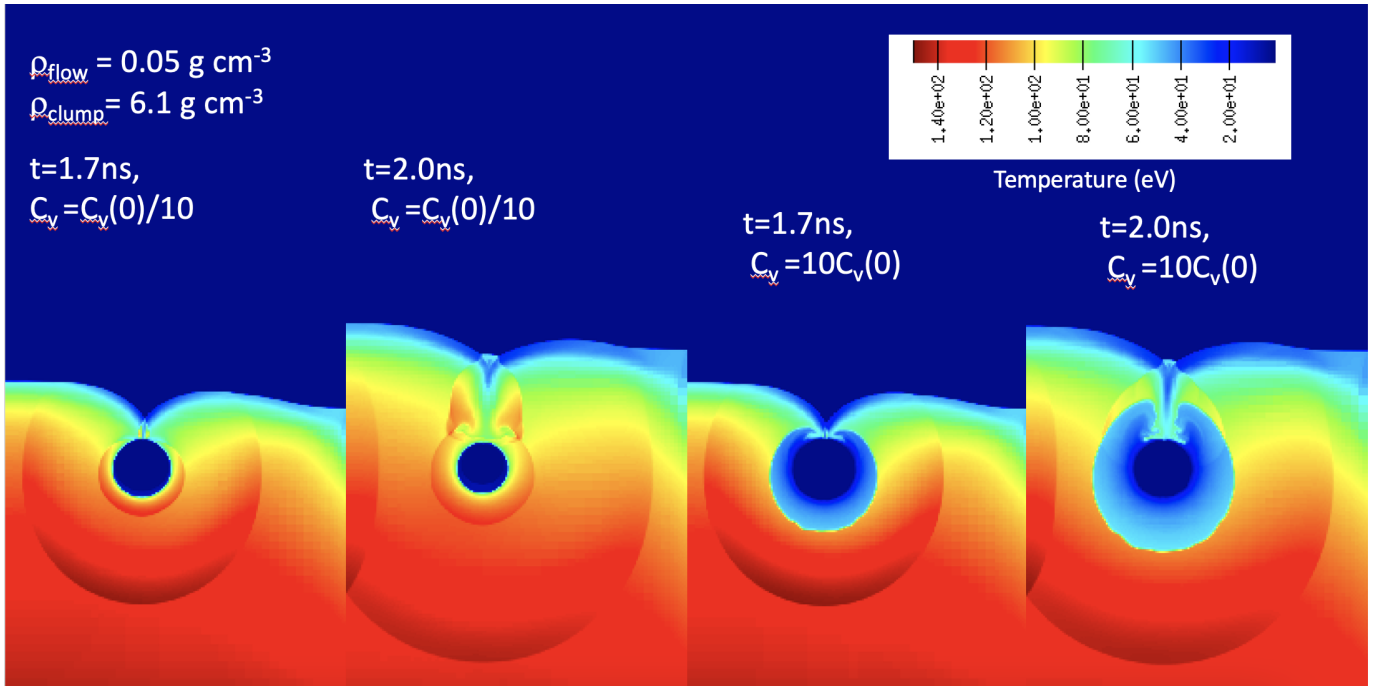


Figure 6. Temperature map for two cylindrical models after 1.7 and 2.0 ns where the specific heat of the clump is lowered and raised by an order of magnitude.

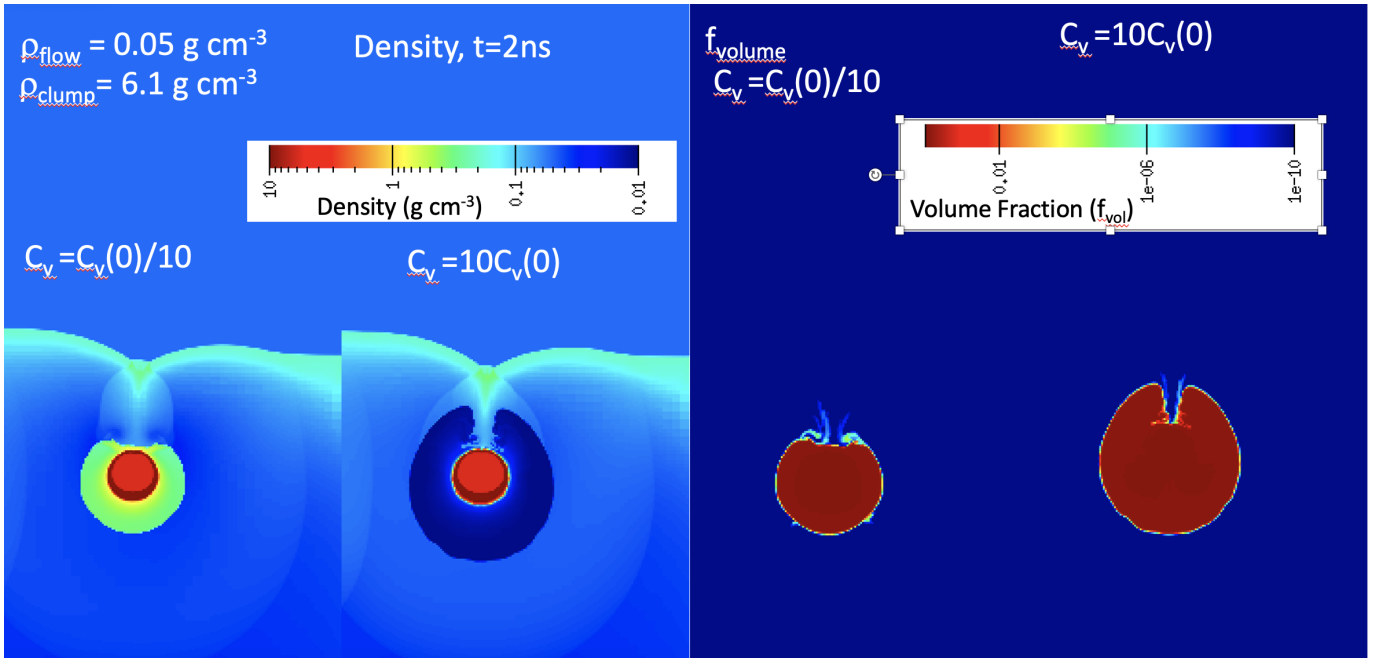


Figure 7. Density and volume fraction (f_{vol}) maps for two cylindrical models at 2.0 ns where the specific heat of the clump is lowered and raised by an order of magnitude. The density of the outflow from the high specific heat clump material is much lower than that of the low specific heat clump material. Because the outflow begins earlier for the high specific heat clump material, its expansion is further out.

therefore has a direct impact on optical spectra [Filinov et al. \(2003\)](#); [Helled et al. \(2020\)](#). A recent study of asymmetric carbon–hydrogen (CH) mixtures has shown that compressing the system to three times its density at $k_B T = 10 \text{ eV}$ results in an almost threefold increase in its electrical and thermal conductivities [White et al. \(2023\)](#). A compressed

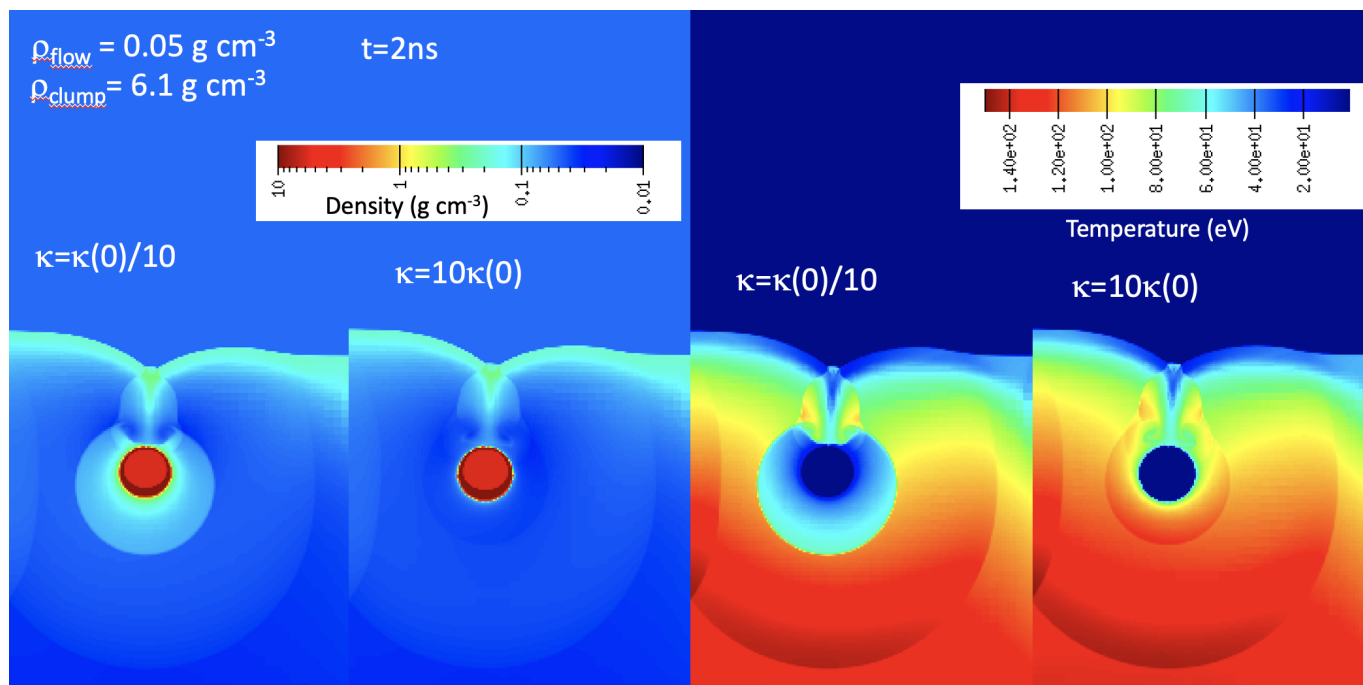


Figure 8. Density and temperature maps for two cylindrical models at 2.0 ns where the opacity of the material in the clump is lowered and raised by an order of magnitude.

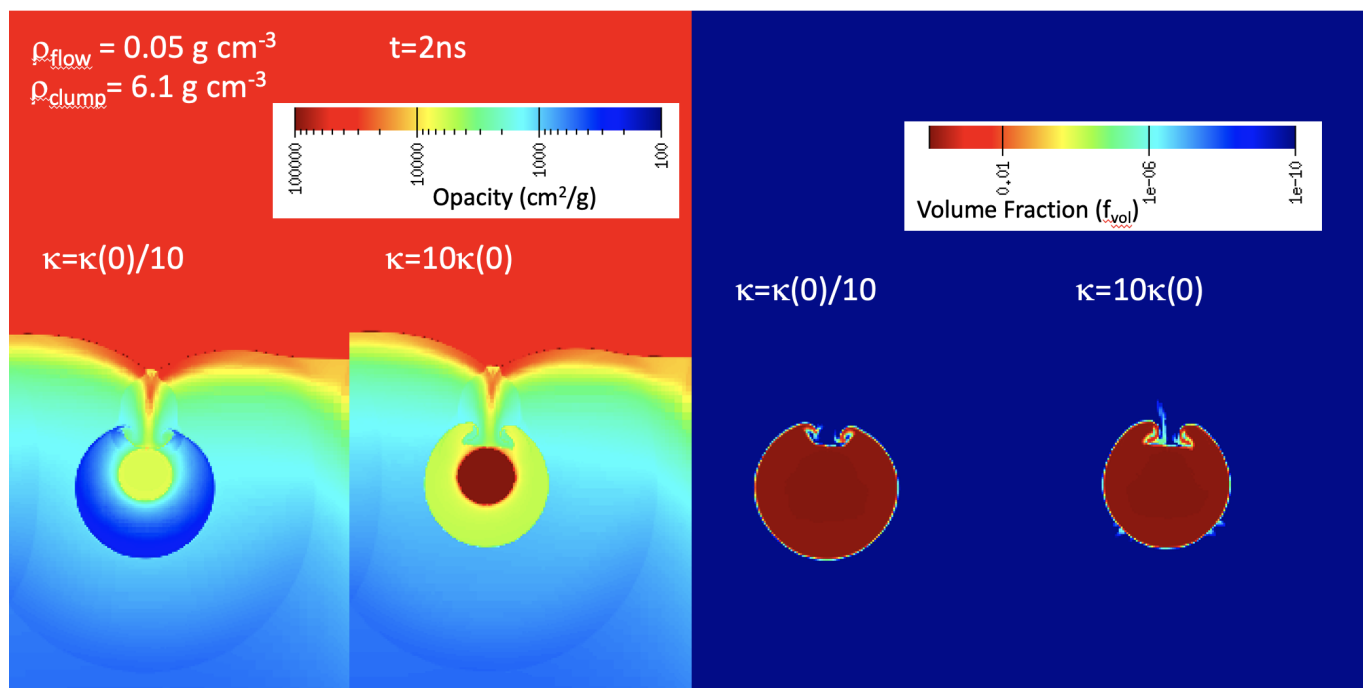


Figure 9. Opacity and volume fraction maps for two cylindrical models at 2.0 ns where the opacity of the material in the clump is lowered and raised by an order of magnitude.

“nonideal” plasma state emerges in numerous dynamic compression environments such as in the laser irradiation of condensed matter in pinched electric discharge experiments, or when the critical density values are attained at high static pressures Boehler (1993); Aquilanti et al. (2015).

In the presence of spatial inhomogeneities, a subtle interplay exists between the temperature gradient arising from thermal conduction and the density profile that evolves to compensate for the thermal gradient [Ping et al. \(2015\)](#). At an inhomogeneous interface, different opacities create a temperature gradient at the junction driving a density gradient. The response of the density to this induced temperature change can serve as a diagnostic tool for thermal conductivity, a critical parameter for planetary modeling.

In these studies, we have assumed numerical issues (e.g. grid resolution, radiation transport methods) do not significantly alter our results. Our standard simulations are fairly high resolution (in a $0.04\text{ cm} = 400\text{ }\mu\text{m}$ target, our resolution is $0.6\text{ }\mu\text{m}$). However, ideally, our calculations would resolve the mean free path of the radiation and typical mean free paths in our clump are $0.15\text{ }\mu\text{m}$. To test the resolution in our standard calculations, we ran a series of high-resolution calculations where the resolution was $0.15\text{ }\mu\text{m}$. The results, comparing the standard- to high-resolution calculations is shown in [Figure 10](#). Although small structures seem to be appearing at $t = 2\text{ ns}$, the outflow and shock positions are identical in these calculations.

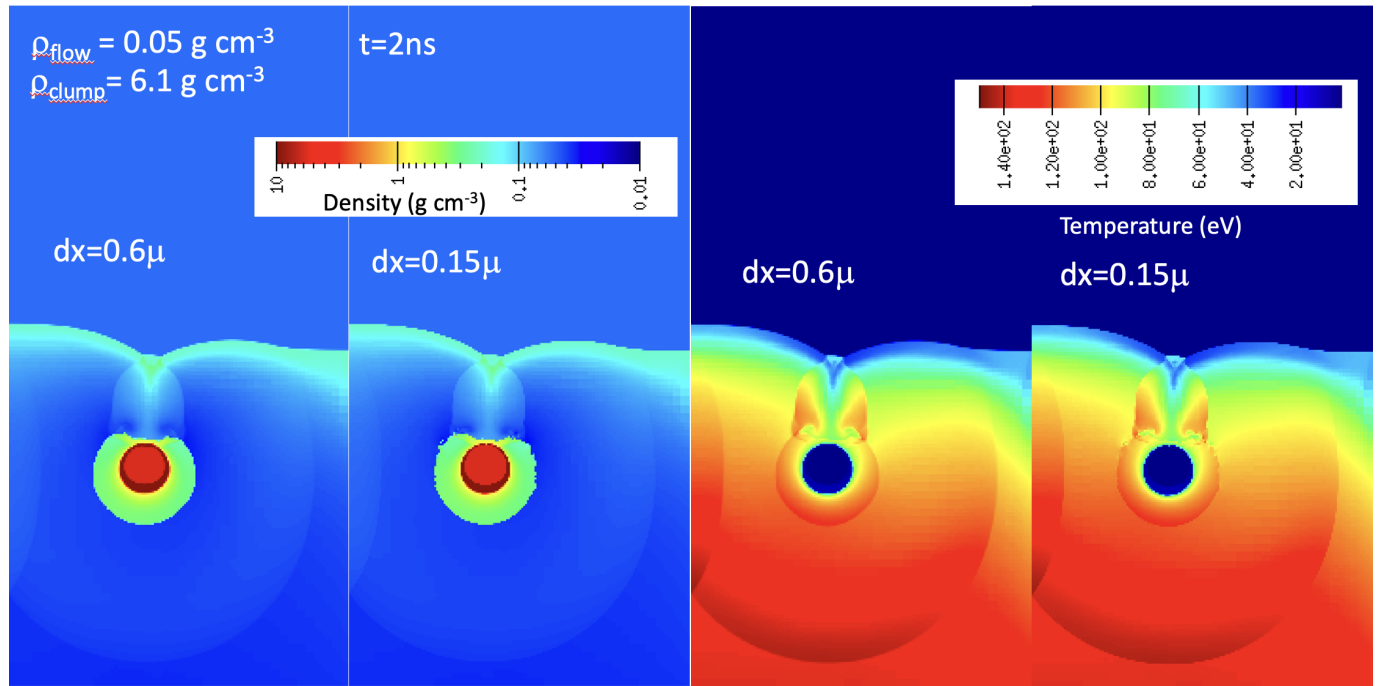


Figure 10. Density and temperature maps for two cylindrical models at 2.0 ns where the resolution is varied by a factor of four (16 times more zones in 2-dimensions).

Another numerical uncertainty lies in the implementation of the radiation transport. As discussed in [Section 4.1](#), the Cassio code includes two higher-order transport methods: discrete ordinate S_N and IMC methods. These two approaches use very different mathematical representations of the angular distribution of the photons and the radiation transport. For most of our calculations, we use the discrete ordinate method. [Figure 11](#) shows the results of this IMC run. The IMC boundary condition is slightly different than that used in the S_N calculations and the angular distribution of the radiation will be slightly different. Comparing to the results in [Figure 10](#), we note that, although there are differences in the sourcing and in the radiation/material coupling algorithms that deposit energy in the zones, the interaction with the clump and its outflow is very similar between the IMC and S_N calculations.

One numerical issue that might lead to differences, but that we do not test here, is the implementation of the hydrodynamics. For instance, the Cassio code uses an adaptive mesh refinement (we only do 2 levels of refinement). We do not compare our results to a Lagrangian hydrodynamics scheme.

In some scenarios, the radiation in the flow can cause the clumps to collapse. For example, in star-forming regions, radiation pressure causes clumps that are on the boundary of gravitational stability to begin to collapse, seeding star formation ([Klein et al. 1980](#)). Radiation pressure also drives the implosion of capsules in inertial confinement fusion ([Lindl 1995](#)). The exact details of the collapse depend on the amount of energy injection versus the radiation

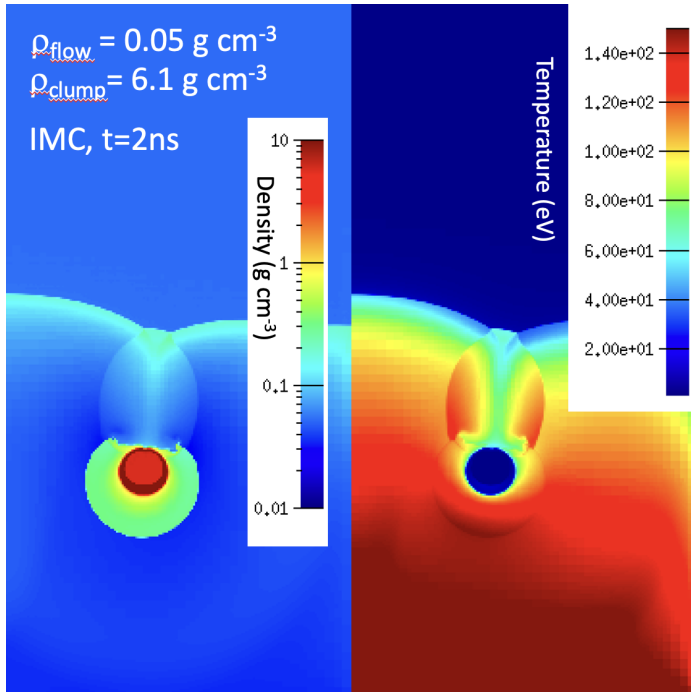


Figure 11. Density and temperature maps for our standard cylindrical model at 2.0 ns using Implicit Monte Carlo. Compare these results to Figure 10. Despite mild differences in initial conditions and large differences in the numerical approaches, the interaction with the clump with these two schemes is very similar.

pressure. As this subject matter diverges from the primary focus of the studies here, we will defer this discussion and detailed study to a later paper.

4.3. Multi-Clump Studies: Putting it all Together

Realistic inhomogeneous radiation-flow problems typically involve chaotic inhomogeneities with many dense clumps. To understand better how radiation flows through a multi-clump medium, we expand our study to include a series of calculations with 25 clumps in our flow region (Byvank et al. 2024) varied the size and number of clumps in a similar experimental setup). To better understand the additional complexity caused by this structure, we have run a series of randomly spaced multi-clump calculations. We continue to use the clump properties (density, composition) from the XFOL and XFLOWS laboratory experiments (Johns et al. 2023; Byvank et al. 2024). We then vary the number, size and distribution of the clumps to better understand the broader implications of inhomogeneous radiation flow. In particular, these studies allow us to investigate the effects of blow-off (and its dependence on the radiation pressure) under more realistic conditions.

For our first study, we focus on the impact of hydrodynamic feedback on the flow of radiation. Figure 12 shows the temperature profile of the same initial clump profile, but with two different drives, each comparing a simulation that is pure transport (“no hydro”) with another that includes hydrodynamic feedback. The pure-transport calculations show an extreme limit where the radiation simply flows around the clumps. For the lower drives, the hydrodynamic feedback is faster than the flow timescale and the clumps expand to block the radiation flow. The radiation flow is dramatically altered by the blow-off from the clumps. With a stronger drive, the outflow is minimized due to both higher radiation pressures and the fact that the flow is faster, allowing less time for hydrodynamic feedback. In the stronger-drive simulations, the differences between the pure-transport and radiation-hydrodynamics simulations are less dramatic.

Because the radiation flow is strongly affected by the clumps in the material-pressure dominated regime, the flow of radiation strongly depends on the distribution of the clumps (in the low clump-number regime). We have run 100 different 25-clump calculations, studying the flow of radiation. Figure 13 compares the time it takes for the radiation to emerge from the clump region for 100 distinct simulations, assuming a random distribution of clumps but conserving

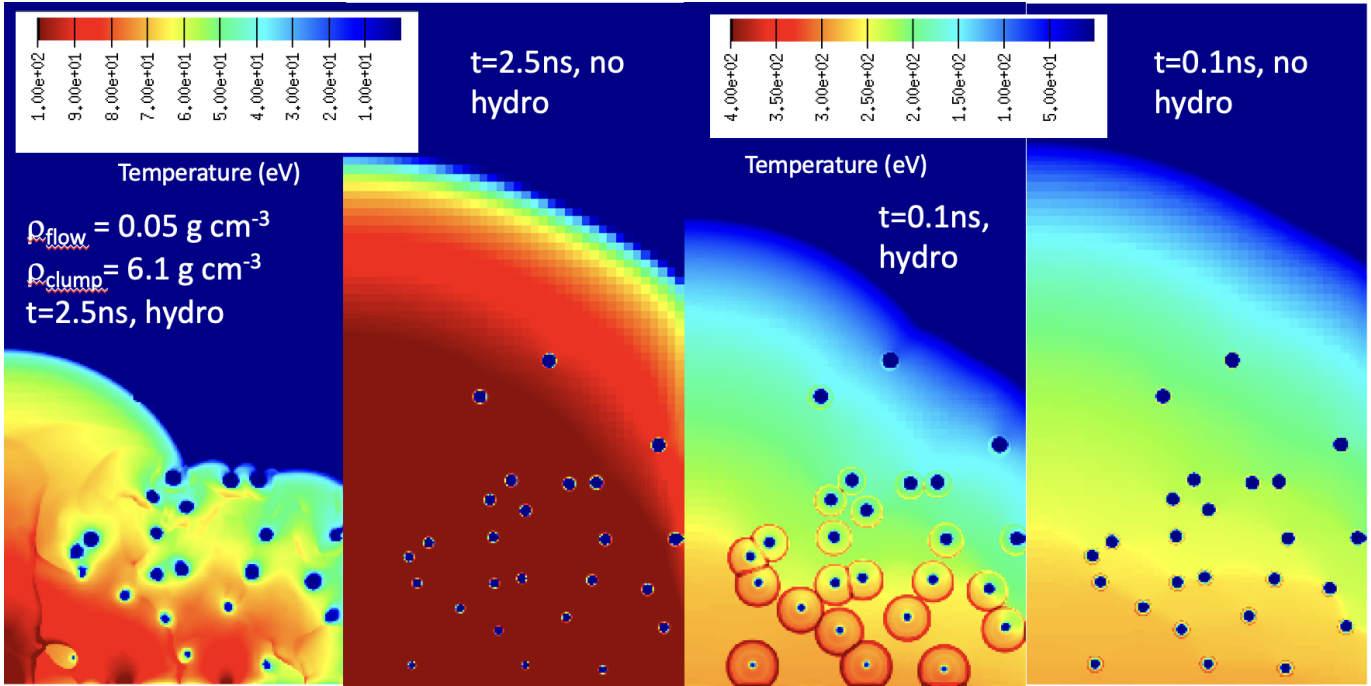


Figure 12. Temperature maps for four cylindrical models with 25 material clumps randomly spaced in the flow region. We use our standard clump and flow densities and compare the solution with and without hydrodynamics turned on. We also vary the temperature of the drive. At our standard temperatures, radiative feedback dramatically alters the flow, but, as we increase the temperature, the differences between pure radiation (“no hydro”) and radiation-hydrodynamics simulations become smaller.

coverage area. The propagation timescale of the radiation front varies by 20%. For many inhomogeneous flows, it will be difficult to exactly characterize the inhomogeneities and any solution will be limited by this uncertainty.

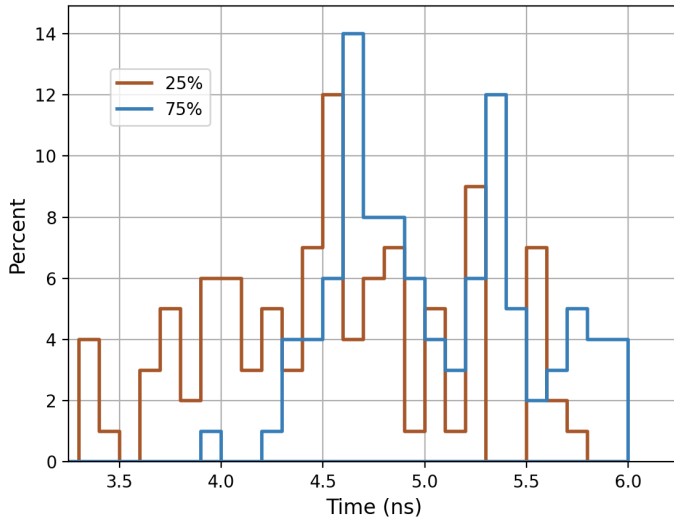


Figure 13. Distribution of radiation-flow timescales for 100 simulations of 25-clump simulations using our standard clump properties ($\rho = 6.1\text{ g cm}^{-3}$, $10\text{ }\mu\text{m}$ diameter), drive power and flow region conditions. The two distributions correspond to the timescale required for a temperature of 25% or 75% of the radiation front at 0.05 cm above the clumpy medium to rise above 20 eV . The spread in the distribution is high (over 2 ns , $> 20\%$) and, at least for these 100 simulations, does not appear to be well-matched by a Gaussian.

The complex structures are very important in our standard models where the radiation temperature is ~ 100 eV and the material pressure of the clumps (after being heated by the radiation) exceeds the radiation pressure. We have run a series of simulations using a high-temperature radiation source where the radiation temperature is at 1 keV. At these temperatures, radiation pressure dominates, simplifying the radiation flow. However, the physics is still much more complex than simple pressure-equilibrium physics suggests or than the subgrid models discussed in Section 3.1 assume. Figure 14 shows the material and radiation pressure of two 100-clump, high-temperature simulations. First note that the radiation and material temperatures are very different for these two models. At these high temperatures, the radiation front moves through our target much faster than the material can equilibrate. Even without this equilibration, blow-off from the clumps still affects the long-term flow.

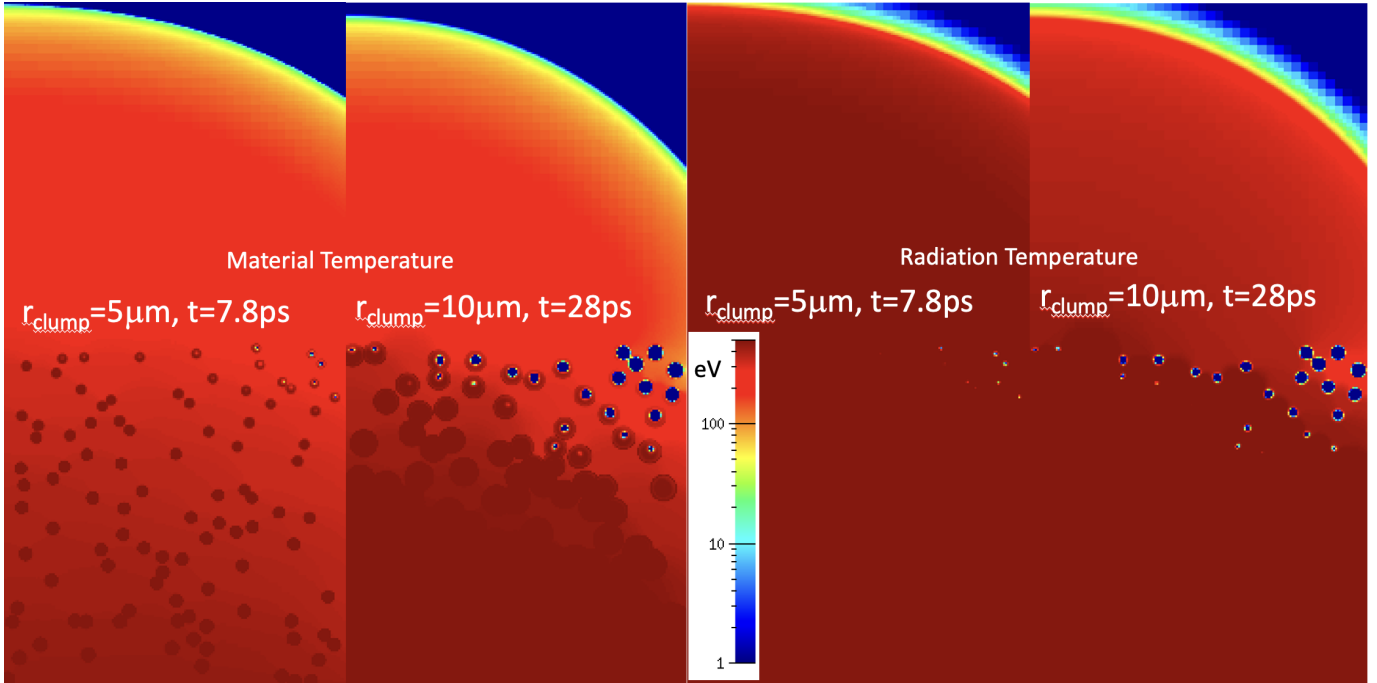


Figure 14. Material and radiation temperature for two 100-clump calculations where the radiation temperature drive is 1 keV. The two calculations use two different clump sizes ($r_{\text{clump}} = 0.05\mu\text{m}, 0.1\mu\text{m}$). The corresponding clump covering fractions of these two models are 5 and 20%. We plot the radiation fronts as they reach the edge of our simulation grid, at 7.8 ps and 28 ps for the small and large clumps, respectively.

For our clump and flow region compositions, as well as for a fixed density and temperature, we expect the clump opacity to only be a factor of 4 higher than the opacity in the flow region. As such, following the prescriptions in Section 3.1, we do not expect such a dramatic effect on the propagation timescale. A few factors contribute to this seeming discrepancy. First, the material temperatures of the clumps and the flow region are not the same (especially just as the radiation front propagates across the clumps) and this difference becomes larger for larger clumps. This can lead to a much more dramatic variation between the clump and flow-region opacities (Figure 15).

The opacities for our materials vary dramatically with temperature and this variation is at the heart of the differences between our simulation results and those of the past analytic prescriptions described in Section 3.1. Because the temperature in the clumps evolves differently than that of the flow region, even if the opacities of the materials are very similar at the same temperature, the opacities for the clump vs. flow region can be very different if their temperatures are different. Especially near the radiation front, the opacities can differ by more than two orders of magnitude. In addition, even though the radiation pressure dominates, the clumps do expand and begin to constrain the entire flow region (Figure 15). If we were only interested in the instantaneous speed of the front, this expansion might not matter. But in steady-state cases, or cases where the front is driven by further radiation, this clump expansion will alter the radiation flow in this inhomogeneous medium.

To further understand the role of clumps, we include two more sets of calculations. In Figure 16, we show the results of three multi-clump calculations, varying the clump number from 25 to nearly 100 clumps. This set of calculations

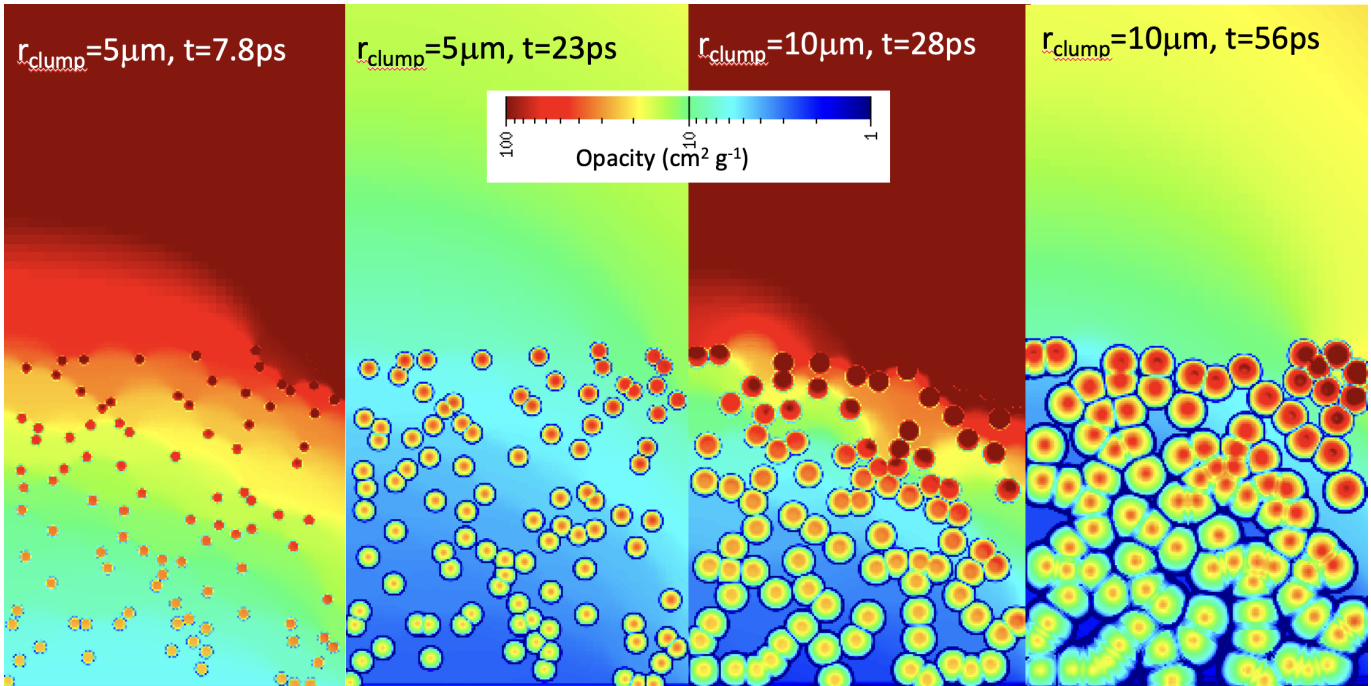


Figure 15. Opacities for the two models from Figure 14 displayed at the two times given in that figure, as well as an intermediate time and a later time, to illustrate the evolution of this opacity with time. Note that the opacity evolves dramatically with time as the material heats, but the clump opacity evolves much more slowly than that of the flow region. Also note that, although this is a radiation-dominated flow, the clumps expand and, for the larger clump size, the clump opacities quickly fill most of the region.

effectively shows the effect of raising the covering fraction from 11% to 44%. Although the basic trends follow what we expect from our subgrid prescriptions, the opacity evolution and expansion factors exacerbate the effects. Another way to understand the deviations from our simple subgrid models is to compare the results of two models with the same clump covering fractions, but different size and number of clumps (Figure 17). Although the covering fraction is initially identical between these two runs, the evolution of the radiation fronts are very different. This behavior is primarily due to the fact that even a small amount of outflow from the clumps can constrain the flow of radiation.

Clearly, even in the radiation-dominated case, hydrodynamics effects like outflow/winds will be important. The subgrid formulae in Section 3.1 will struggle to match this data. The Sundqvist et al. (2018) formulae discussed in Section 3.1 do not reproduce the magnitude of this variation. Although the additional scattering term in the Olson (2007) approach can come closer to fitting the data, this requires incorporating the temperature-dependence of the opacity. We defer a detailed application-specific comparison of these subgrid models to a later paper.

5. APPLICATIONS REVISITED

Radiation flow through inhomogeneous media is critical for a broad range of problems in astrophysics and beyond (see Table 1). In many cases, the inhomogeneities can not be resolved in the large-scale calculations of these applications. In this paper, we reviewed some of the recipes developed to capture radiation transport through these media and the experiments developed to test them.

This paper included a large set of simulations to better understand the physics behind radiation flow through an inhomogeneous medium. We found that for regimes where the radiation pressure is not dominant, radiative heating of the high-density clumps can cause the clumps to expand. This wind can increase the opacity throughout the medium, dramatically altering the flow of radiation. Most of the recipes in the literature focus on transport-only effects, which are more valid for the conditions where radiation pressure dominates. But, as we have seen in this paper, even in a radiation-pressure dominated system, radiation-hydrodynamics effects can not be ignored.

In all of our models, energy deposition from the radiation front played a much bigger role than momentum deposition and hence, “outflows” or “winds” were more important for the subsequent evolution than ablation. For less dense clumps, as we might expect from turbulent instabilities, ablation can play a much more important role Fryer et al.

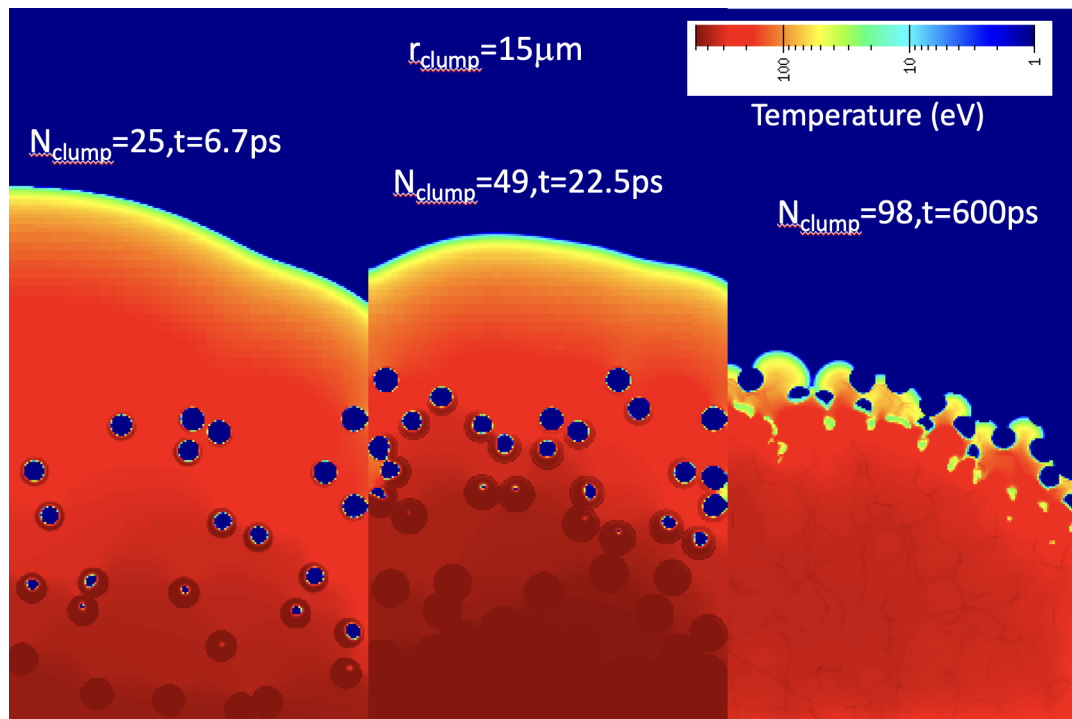


Figure 16. Temperature of a strong-drive radiation flow through a clumpy medium where the clump radius is $15\ \mu\text{m}$ and the number of clumps varies from 25 to 98. As the covering fraction increases, the radiation timescale for the propagation of the radiation front increases dramatically and the times for each panel are very different.

(2020a). Ablation will have a similar effect to blow-off in the sense that it will disperse the clumpy material, causing shocks and cutting off the flow. But the nature of ablation will be different than the models shown here and much more work must be done to understand all aspects of inhomogeneous radiation flow for the broad set of applications discussed in this paper.

We noted the complications caused by opacities that vary rapidly with temperature. For our materials, the opacity for both our materials drops by over an order of magnitude as the radiation front propagates across the flow region. The opacity of the clump material will drop much slower because it takes time for it to heat. The same is true for many astrophysical conditions. Figure 18 shows the solar opacities from the Los Alamos OPLIB database for a range of temperatures and densities. The temperature of a giant star is roughly 10,000 K, but can rise up to 1 million K when the supernova blastwave breaks out of the star. In such scenarios, that opacity can drop as much as 3 orders of magnitude. Any subgrid model estimating the opacities of a clumpy medium must include this temperature dependence. This figure assumes the radiation and matter are in equilibrium. As we showed in our simulations, it is unlikely that this will hold in many applications. Out-of-equilibrium effects must be included to fully follow this radiation flow.

At this time, the physics is sufficiently complex that no model captures all of these effects. A much more comprehensive study is needed to develop a more generic solution and it may be that the more appropriate approach would be to devise individual recipes for specific problems. We defer this study to a later paper.

- 1 The work by CLF was supported by the US Department of Energy through the Los Alamos National Laboratory.
- 2 Los Alamos National Laboratory is operated by Triad National Security, LLC, for the National Nuclear Security
- 3 Administration of U.S. Department of Energy (Contract No. 89233218CNA000001). A portion of the work by CLF
- 4 was performed at the Aspen Center for Physics, which is supported by National Science Foundation grant PHY-
- 5 1607611.

REFERENCES

- Aquilanti, G., Trapananti, A., Karandikar, A., et al. 2015, Proceedings of the National Academy of Sciences, 112, 12042, doi: [10.1073/pnas.1502363112](https://doi.org/10.1073/pnas.1502363112)
- Bayless, A. J., Even, W., Frey, L. H., et al. 2015, ApJ, 805, 98, doi: [10.1088/0004-637X/805/2/98](https://doi.org/10.1088/0004-637X/805/2/98)

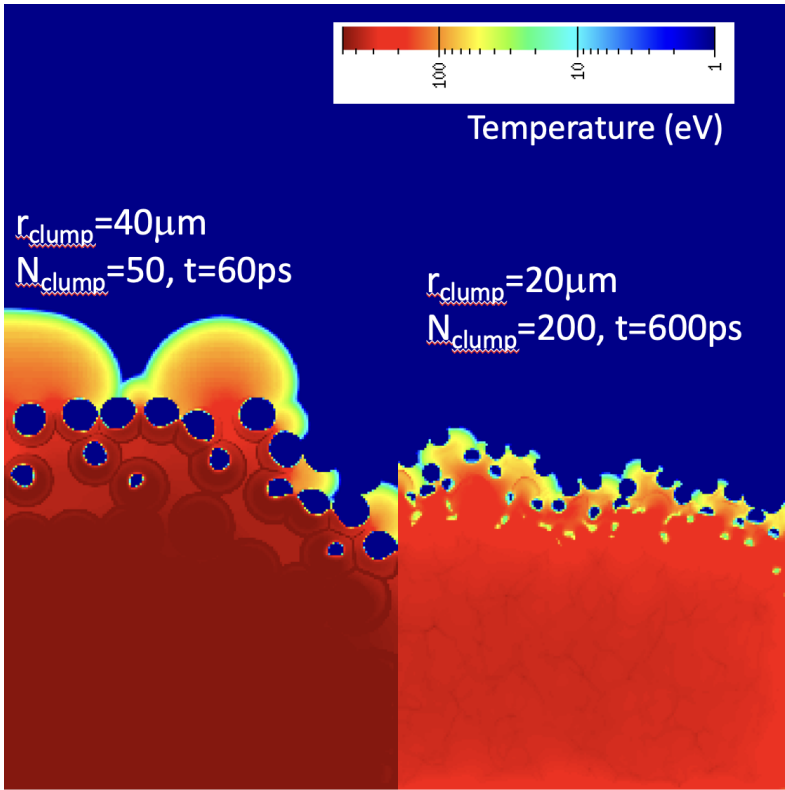


Figure 17. Temperature of a strong-drive radiation flow through a clumpy medium where the clump radius and number of clumps are modified to produce the same covering fraction. Comparing to Figure 16 demonstrates the importance of the clump size on the radiation flow.

- Bisbas, T. G., Wünsch, R., Whitworth, A. P., Hubber, D. A., & Walch, S. 2011, *ApJ*, 736, 142, doi: [10.1088/0004-637X/736/2/142](https://doi.org/10.1088/0004-637X/736/2/142)
- Boehler, R. 1993, *Nature*, 363, 534, doi: [10.1038/363534a0](https://doi.org/10.1038/363534a0)
- Boehly, T. R., Craxton, R. S., Hinterman, T. H., et al. 1995, *Review of Scientific Instruments*, 66, 508, doi: [10.1063/1.1146333](https://doi.org/10.1063/1.1146333)
- Boisse, P. 1990, *A&A*, 228, 483
- Brantley, P. S. 2011, *JQSRT*, 112, 599, doi: [10.1016/j.jqsrt.2010.06.007](https://doi.org/10.1016/j.jqsrt.2010.06.007)
- Bustard, C., & Zweibel, E. G. 2021, *ApJ*, 913, 106, doi: [10.3847/1538-4357/abf64c](https://doi.org/10.3847/1538-4357/abf64c)
- Byvank et al., i. p. 2024, in preparation
- Coffing, S. X., Fryer, C. L., Robey, H. F., et al. 2022, *Physics of Plasmas*, 29, 083302, doi: [10.1063/5.0081167](https://doi.org/10.1063/5.0081167)
- Colgan, J., Kilcrease, D. P., Magee, N. H., et al. 2016, *ApJ*, 817, 116, doi: [10.3847/0004-637X/817/2/116](https://doi.org/10.3847/0004-637X/817/2/116)
- Cook, P. A., de Oliveira, C. R. E., Haigh, J. D., & Goddard, A. J. 2004, *Atmospheric Research*, 72, 223, doi: [10.1016/j.atmosres.2004.03.021](https://doi.org/10.1016/j.atmosres.2004.03.021)
- Davis, A. B., & Xu, F. 2014, arXiv e-prints, arXiv:1410.8200, doi: [10.48550/arXiv.1410.8200](https://doi.org/10.48550/arXiv.1410.8200)
- Falk, K., McCoy, C. A., Fryer, C. L., et al. 2014, *PhRvE*, 90, 033107, doi: [10.1103/PhysRevE.90.033107](https://doi.org/10.1103/PhysRevE.90.033107)
- Falk, K., Fryer, C. L., Gamboa, E. J., et al. 2017, *Plasma Physics and Controlled Fusion*, 59, 014050, doi: [10.1088/0741-3335/59/1/014050](https://doi.org/10.1088/0741-3335/59/1/014050)
- Falk, K., Holec, M., Fontes, C. J., et al. 2018, *PhRvL*, 120, 025002, doi: [10.1103/PhysRevLett.120.025002](https://doi.org/10.1103/PhysRevLett.120.025002)
- . 2020a, *PhRvL*, 124, 159901, doi: [10.1103/PhysRevLett.124.159901](https://doi.org/10.1103/PhysRevLett.124.159901)
- Falk, K., Fontes, C. J., Fryer, C. L., et al. 2020b, *Plasma Physics and Controlled Fusion*, 62, 074001, doi: [10.1088/1361-6587/ab8bb3](https://doi.org/10.1088/1361-6587/ab8bb3)
- Fatenejad, M., Fryxell, B., Wohlbiel, J., et al. 2013, *High Energy Density Physics*, 9, 63, doi: [10.1016/j.hedp.2012.10.004](https://doi.org/10.1016/j.hedp.2012.10.004)
- Filinov, V. S., Bonitz, M., Levashov, P., et al. 2003, *Journal of Physics A: Mathematical and General*, 36, 6069, doi: [10.1088/0305-4470/36/22/332](https://doi.org/10.1088/0305-4470/36/22/332)
- Fontes, C. J., Zhang, H. L., Abdallah, Jr., J., et al. 2015, *Journal of Physics B Atomic Molecular Physics*, 48, 144014, doi: [10.1088/0953-4075/48/14/144014](https://doi.org/10.1088/0953-4075/48/14/144014)
- Fryer, C. L., Fontes, C. J., Warsa, J. S., et al. 2020a, *ApJ*, 898, 123, doi: [10.3847/1538-4357/ab99a7](https://doi.org/10.3847/1538-4357/ab99a7)
- Fryer, C. L., Rockefeller, G., & Young, P. A. 2006, *ApJ*, 647, 1269, doi: [10.1086/505590](https://doi.org/10.1086/505590)

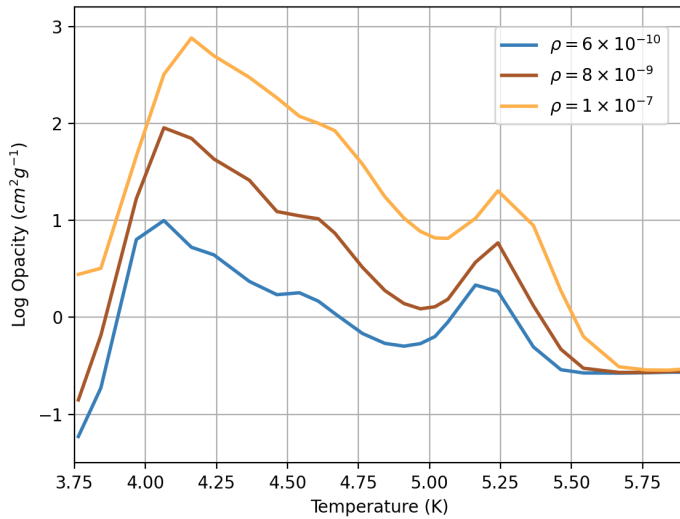


Figure 18. OPLIB opacities versus temperature for solar-abundance material near the edge of a massive star corresponding to the conditions during the onset of shock breakout. The opacity can drop over three orders of magnitude as the temperature rises from 10,000 K to a few 100,000 K.

- Fryer, C. L., Diaw, A., Fontes, C. J., et al. 2020b, *High Energy Density Physics*, 35, 100738, doi: [10.1016/j.hedp.2019.100738](https://doi.org/10.1016/j.hedp.2019.100738)
- Fryer, C. L., Wood, S., Coffing, S. X., et al. 2023, *High Energy Density Physics*, 46, 101023, doi: [10.1016/j.hedp.2022.101023](https://doi.org/10.1016/j.hedp.2022.101023)
- Gittings, M., Weaver, R., Clover, M., et al. 2008, *Computational Science and Discovery*, 1, 015005, doi: [10.1088/1749-4699/1/1/015005](https://doi.org/10.1088/1749-4699/1/1/015005)
- Haynam, C. A., Wegner, P. J., Auerbach, J. M., et al. 2007, *ApOpt*, 46, 3276, doi: [10.1364/AO.46.003276](https://doi.org/10.1364/AO.46.003276)
- Hegmann, M., & Kegel, W. H. 2003, *MNRAS*, 342, 453, doi: [10.1046/j.1365-8711.2003.06543.x](https://doi.org/10.1046/j.1365-8711.2003.06543.x)
- Helled, R., Mazzola, G., & Redmer, R. 2020, *Nature Reviews Physics*, 2, 562, doi: [10.1038/s42254-020-0223-3](https://doi.org/10.1038/s42254-020-0223-3)
- Herwig, F., Woodward, P. R., Lin, P.-H., Knox, M., & Fryer, C. 2014, *ApJL*, 792, L3, doi: [10.1088/2041-8205/792/1/L3](https://doi.org/10.1088/2041-8205/792/1/L3)
- Hogan, R. J., Schäfer, S. A. K., Klinger, C., Chiu, J. C., & Mayer, B. 2016, *Journal of Geophysical Research (Atmospheres)*, 121, 8583, doi: [10.1002/2016JD024875](https://doi.org/10.1002/2016JD024875)
- Huang, X., Jiang, Y.-f., & Davis, S. W. 2022, *ApJ*, 931, 140, doi: [10.3847/1538-4357/ac69dc](https://doi.org/10.3847/1538-4357/ac69dc)
- Irwin, C. M., Linial, I., Nakar, E., Piran, T., & Sari, R. 2021, *MNRAS*, 508, 5766, doi: [10.1093/mnras/stab2705](https://doi.org/10.1093/mnras/stab2705)
- Jiang, Y.-F., Cantiello, M., Bildsten, L., et al. 2018, *Nature*, 561, 498, doi: [10.1038/s41586-018-0525-0](https://doi.org/10.1038/s41586-018-0525-0)
- Joggerst, C. C., Nelson, A., Woodward, P., et al. 2014, *Journal of Computational Physics*, 275, 154, doi: [10.1016/j.jcp.2014.06.037](https://doi.org/10.1016/j.jcp.2014.06.037)
- Johns, H. M., Lanier, N. E., Kline, J. L., et al. 2016, *Review of Scientific Instruments*, 87, 11E337, doi: [10.1063/1.4962195](https://doi.org/10.1063/1.4962195)
- Johns, H. M., Fryer, C. L., Wood, S. R., et al. 2021, *High Energy Density Physics*, 39, 100939, doi: [10.1016/j.hedp.2021.100939](https://doi.org/10.1016/j.hedp.2021.100939)
- Johns, H. M., Byvank, T., Robey, H., et al. 2023, *Review of Scientific Instruments*, 94, 023502, doi: [10.1063/5.0101421](https://doi.org/10.1063/5.0101421)
- Kassianov, E. 2003, *JQSRT*, 77, 373, doi: [10.1016/S0022-4073\(02\)00170-X](https://doi.org/10.1016/S0022-4073(02)00170-X)
- Keiter, P., Gunderson, M., Foster, J., et al. 2008, *Physics of Plasmas*, 15, 056901, doi: [10.1063/1.2927529](https://doi.org/10.1063/1.2927529)
- Klein, R. I., Sandford, M. T., I., & Whitaker, R. W. 1980, *SSRv*, 27, 275, doi: [10.1007/BF00168309](https://doi.org/10.1007/BF00168309)
- Larmier, C., Mazzola, A., Zoia, A., Lemaire, S., & Riz, D. 2021, in *European Physical Journal Web of Conferences*, Vol. 247, *European Physical Journal Web of Conferences*, 04009, doi: [10.1051/epjconf/202124704009](https://doi.org/10.1051/epjconf/202124704009)
- Lindl, J. 1995, *Physics of Plasmas*, 2, 3933, doi: [10.1063/1.871025](https://doi.org/10.1063/1.871025)
- Lovegrove, E., Woosley, S. E., & Zhang, W. 2017, *ApJ*, 845, 103, doi: [10.3847/1538-4357/aa7b7d](https://doi.org/10.3847/1538-4357/aa7b7d)
- Malvagi, F., Levermore, C. D., & Pomraning, G. C. 1989, *Transport Theory and Statistical Physics*, 18, 287, doi: [10.1080/00411458908204690](https://doi.org/10.1080/00411458908204690)
- Miller, D. S., Graziani, F., & Rodrigue, G. 2001, *JQSRT*, 70, 115, doi: [10.1016/S0022-4073\(00\)00128-X](https://doi.org/10.1016/S0022-4073(00)00128-X)
- Olson, G. L. 2007, *JQSRT*, 104, 86, doi: [10.1016/j.jqsrt.2006.08.013](https://doi.org/10.1016/j.jqsrt.2006.08.013)

- Olson, G. L., Miller, D. S., Larsen, E. W., & Morel, J. E. 2006, *JQSRT*, 101, 269, doi: [10.1016/j.jqsrt.2005.11.070](https://doi.org/10.1016/j.jqsrt.2005.11.070)
- Owocki, S. P., Hirai, R., Podsiadlowski, P., & Schneider, F. R. N. 2019, *MNRAS*, 485, 988, doi: [10.1093/mnras/stz461](https://doi.org/10.1093/mnras/stz461)
- Owocki, S. P., & Rybicki, G. B. 1984, *ApJ*, 284, 337, doi: [10.1086/162412](https://doi.org/10.1086/162412)
- Owocki, S. P., & Sundqvist, J. O. 2018, *MNRAS*, 475, 814, doi: [10.1093/mnras/stx3225](https://doi.org/10.1093/mnras/stx3225)
- Ping, Y., Fernandez-Panella, A., Sio, H., et al. 2015, *Physics of Plasmas*, 22, 092701, doi: [10.1063/1.4929797](https://doi.org/10.1063/1.4929797)
- Pomraning, G. 1998, *Journal of Quantitative Spectroscopy and Radiative Transfer*, 60, 181
- Prinja, A. K., & Olson, G. L. 2005, *JQSRT*, 90, 131, doi: [10.1016/j.jqsrt.2004.03.010](https://doi.org/10.1016/j.jqsrt.2004.03.010)
- Proga, D., Jiang, Y.-F., Davis, S. W., Stone, J. M., & Smith, D. 2014, *ApJ*, 780, 51, doi: [10.1088/0004-637X/780/1/51](https://doi.org/10.1088/0004-637X/780/1/51)
- Puls, J., Vink, J. S., & Najjarro, F. 2008, *A&A Rv*, 16, 209, doi: [10.1007/s00159-008-0015-8](https://doi.org/10.1007/s00159-008-0015-8)
- Quataert, E., Fernández, R., Kasen, D., Klion, H., & Paxton, B. 2016, *MNRAS*, 458, 1214, doi: [10.1093/mnras/stw365](https://doi.org/10.1093/mnras/stw365)
- Roming, P. W. A., Pritchard, T. A., Prieto, J. L., et al. 2012, *ApJ*, 751, 92, doi: [10.1088/0004-637X/751/2/92](https://doi.org/10.1088/0004-637X/751/2/92)
- Sandford, M. T., I., Whitaker, R. W., & Klein, R. I. 1982, *ApJ*, 260, 183, doi: [10.1086/160245](https://doi.org/10.1086/160245)
- Shabanov, N. V., Huang, D., Knjazikhin, Y., Dickinson, R. E., & Myneni, R. B. 2007, *JQSRT*, 107, 236, doi: [10.1016/j.jqsrt.2007.01.053](https://doi.org/10.1016/j.jqsrt.2007.01.053)
- Shaoen, J., Yan, X., Yongkun, D., et al. 2005, *Plasma Science and Technology*, 7, 2965
- Smith, C. C. 2003, *JQSRT*, 81, 451, doi: [10.1016/S0022-4073\(03\)00095-5](https://doi.org/10.1016/S0022-4073(03)00095-5)
- Su, B., & Pomraning, G. C. 1994, *JQSRT*, 51, 467, doi: [10.1016/0022-4073\(94\)90147-3](https://doi.org/10.1016/0022-4073(94)90147-3)
- . 1995, *JQSRT*, 54, 779, doi: [10.1016/0022-4073\(95\)00110-7](https://doi.org/10.1016/0022-4073(95)00110-7)
- Sundqvist, J. O., Owocki, S. P., & Puls, J. 2018, *A&A*, 611, A17, doi: [10.1051/0004-6361/201731718](https://doi.org/10.1051/0004-6361/201731718)
- Sundqvist, J. O., Puls, J., & Owocki, S. P. 2014, *A&A*, 568, A59, doi: [10.1051/0004-6361/201423570](https://doi.org/10.1051/0004-6361/201423570)
- Urbatsch, T. J., & Evans, T. M. 2006, *Milagro version 2 an implicit Monte Carlo code for thermal radiative transfer: Capabilities, development, and usage*, Tech. rep., Los Alamos National Lab.(LANL), Los Alamos, NM (United States)
- Vanderhaegen, D. 1986, *JQSRT*, 36, 557, doi: [10.1016/0022-4073\(86\)90128-7](https://doi.org/10.1016/0022-4073(86)90128-7)
- . 1988, *JQSRT*, 39, 333, doi: [10.1016/0022-4073\(88\)90009-X](https://doi.org/10.1016/0022-4073(88)90009-X)
- Vu, E. H., Brantley, P. S., Olson, A. J., & Kiedrowski, B. C. 2020, LLNL report. <https://www.osti.gov/biblio/1824766>
- Waxman, E., & Katz, B. 2017, in *Handbook of Supernovae*, ed. A. W. Alsabti & P. Murdin, 967, doi: [10.1007/978-3-319-21846-5_33](https://doi.org/10.1007/978-3-319-21846-5_33)
- White, A., Craven, G., Sharma, V., & Collins, L. 2023, In preparation for *Physics of Plasmas*
- Wiener, J., Zweibel, E. G., & Ruszkowski, M. 2019, *MNRAS*, 489, 205, doi: [10.1093/mnras/stz2007](https://doi.org/10.1093/mnras/stz2007)
- Witt, A. N., & Gordon, K. D. 1996, *ApJ*, 463, 681, doi: [10.1086/177282](https://doi.org/10.1086/177282)
- . 2000, *ApJ*, 528, 799, doi: [10.1086/308197](https://doi.org/10.1086/308197)
- Wu, X. 2013, in *AGU Fall Meeting Abstracts*, Vol. 2013, A43B–0256
- Ze, F., Kauffman, R., Kilkenny, J., et al. 1992, *Review of scientific instruments*, 63, 5124